Exploring the canonical behaviour of long gamma-ray bursts using an intrinsic multiwavelength afterglow correlation

S. R. Oates,[1,2]★ J. L. Racusin,[3] M. De Pasquale,[1,4] M. J. Page,[1] A. J. Castro-Tirado,[2,5] J. Gorosabel,[2,6,7]† P. J. Smith,[1] A. A. Breeveld[1] and N. P. M Kuin[1]

[1]*Mullard Space Science Laboratory, University College London, Holmbury St. Mary, Dorking, Surrey RH5 6NT, UK*
[2]*Instituto de Astrofsica de Andalucía (IAA-CSIC), Glorieta de la Astronomía s/n, E-18008, Granada, Spain*
[3]*Astrophysics Science Division, NASA Goddard Space Flight Center, 8800 Greenbelt Road, Greenbelt, MD 20771, USA*
[4]*Istituto Astrofisica Spaziale Fisica Cosmica, Via Ugo La Malfa 153, I-90146 Palermo, Italy*
[5]*Unidad Asociada Departamento de Ingeniería de Sistemas y Automática, E.T.S. de Ingenieros Industriales, Universidad de Málaga, E-29071 Málaga, Spain*
[6]*Unidad Asociada Grupo Ciencias Planetarias UPV/EHU-IAA/CSIC, Departamento de Física Aplicada I, E.T.S., Ingeniería, Universidad del País Vasco UPV/EHU, Alameda de Urquijo s/n, E-48013 Bilbao, Spain*
[7]*Ikerbasque, Basque Foundation for Science, Alameda de Urquijo 36-5, E-48008 Bilbao, Spain*

ABSTRACT

In this paper, we further investigate the relationship, reported by Oates et al., between the optical/UV afterglow luminosity (measured at restframe 200 s) and average afterglow decay rate (measured from restframe 200 s onwards) of long duration gamma-ray bursts (GRBs). We extend the analysis by examining the X-ray light curves, finding a consistent correlation. We therefore explore how the parameters of these correlations relate to the prompt emission phase and, using a Monte Carlo simulation, explore whether these correlations are consistent with predictions of the standard afterglow model. We find significant correlations between: $\log L_{O,200\,s}$ and $\log L_{X,200\,s}$; $\alpha_{O,>200\,s}$ and $\alpha_{X,>200\,s}$, consistent with simulations. The model also predicts relationships between $\log E_{iso}$ and $\log L_{200\,s}$; however, while we find such relationships in the observed sample, the slope of the linear regression is shallower than that simulated and inconsistent at $\gtrsim 3\sigma$. Simulations also do not agree with correlations observed between $\log L_{200\,s}$ and $\alpha_{>200\,s}$, or $\log E_{iso}$ and $\alpha_{>200\,s}$. Overall, these observed correlations are consistent with a common underlying physical mechanism producing GRBs and their afterglows regardless of their detailed temporal behaviour. However, a basic afterglow model has difficulty explaining all the observed correlations. This leads us to briefly discuss alternative more complex models.

Key words: gamma-ray burst: general.

1 INTRODUCTION

Gamma-ray bursts (GRBs) are intense flashes of gamma-rays that are usually accompanied by an afterglow, longer lived emission that may be detected at X-ray to radio wavelengths. Studies of single GRBs provide exceptional detail on the behaviour and physical properties of individual events. However, statistical investigations of large samples of GRBs aim to find common characteristics and correlations that link individual events and therefore provide insight into the mechanisms common to GRBs. Statistical investigations performed so far have found a number of trends and correlations within and linking the prompt gamma-ray emission and the afterglow emission (e.g. Amati et al. 2002; Ghirlanda, Ghisellini &

Lazzati 2004; Dainotti, Cardone & Capozziello 2008; Panaitescu & Vestrand 2008; Bernardini et al. 2012; D'Avanzo et al. 2012; Li et al. 2012; Liang et al. 2013; Panaitescu, Vestrand & Woźniak 2013; Zaninoni et al. 2013). Within the prompt gamma-ray emission, the most renowned correlation discovered is the Amati relation, a correlation between the isotropic gamma-ray energy E_{iso} and the rest-frame gamma-ray peak energy E_{peak} (see Amati et al. 2002, and references therein). The exact origin of the correlation is uncertain, but it can be explained by the non-thermal synchrotron model, jets viewed over a range of viewing angles or with jets of different non-uniform structure (Amati 2006) and can also be produced in the photospheric model (Lazzati et al. 2013). Within the afterglow, several trends are apparent and are currently being explored. The simplest observation is that the luminosity light curves, in both the X-ray and optical/UV samples, show clustered behaviour. Evidence for clustering into two groups, at ∼0.5–1 d, for the

★ E-mail: sro@iaa.es
† Deceased.

optical/IR GRB afterglows was reported by Boër & Gendre (2000), Gendre & Boër (2005), Nardini et al. (2006), Liang & Zhang (2006), Nardini, Ghisellini & Ghirlanda (2008) and Gendre et al. (2008). However, several more recently published works have suggested that the afterglow distributions are unimodal (Melandri et al. 2008; Cenko et al. 2009a; Oates et al. 2009; Kann et al. 2010; Melandri et al. 2014).

There has also been a suggestion that in samples of pre-*Swift* X-ray afterglow light curves with bimodal luminosity distributions, the more luminous cluster decays more quickly than the less luminous cluster of X-ray afterglows (Boër & Gendre 2000; Gendre & Boër 2005), implying a possible relationship between the brightness of the GRB afterglow and the rate that it decays. Gendre, Galli & Boër (2008) extended their X-ray afterglow sample to include the first 1.5 yr of *Swift* light curves. Using data from the end of the X-ray plateau phase (between 200 s and 129 ks) onwards, they again observed clustering into two groups (three groups including low-luminosity GRBs), but they could not support previous claims that the brighter cluster of GRBs decay typically faster than the fainter cluster of GRBs.

A relationship between the intrinsic brightness and rate of decay of GRBs has also been explored in other studies. Kouveliotou et al. (2004) explored a sample of 15 X-ray luminosity light curves from a mix of GRBs and supernovae (SNe). With extrapolation of the GRB X-ray light curves to a few thousand days after the trigger, the initially broad luminosity distribution of GRB and SNe light curves narrows with time by an order of magnitude, suggesting the brightest decayed more quickly. In Oates et al. (2009), within a sample of 27 *Swift* Ultra-violet Optical Telescope (UVOT; Roming et al. 2005) afterglow light curves, observed between <400 s and >10^5 s, a correlation was noticed in the observed frame between the magnitude of the v-band afterglow light curve at 400 s and the average rate at which the light curves decayed. A rest-frame correlation proved inconclusive due to the small sample size. The cluster of luminosity light curves in Kann et al. (2010), showed evidence for narrowing of the distribution with time, also suggesting a relationship between the brightness of the afterglow and the rate of decay. In Oates et al. (2012), the UVOT sample was extended to 48 optical/UV GRB light curves. Consistent with Kann et al. (2010) and other studies mention above, the optical/UV luminosity light curves clustered into a single group and it was apparent that the luminosity distribution was wider during the early part of the afterglow, and became narrower as the afterglows faded. This finding suggests that the most luminous GRB afterglows at early epochs, decay more quickly than the less luminous afterglows. Using the logarithmic optical brightness (log $L_{O,200\,s}$; measured at rest frame 200 s and at a rest-frame wavelength 1600 Å), and average decay rate of GRB afterglows ($\alpha_{>200\,s}$; measured from rest frame 200 s onwards with a single power law and thus ignoring the precise temporal behaviour of the afterglow), Oates et al. (2012) tested to see if this correlation was statistically significant. With a Spearman rank test a coefficient of −0.58 at a significance of 99.998 per cent (4.2σ) was found, indicating that these two parameters are correlated. This correlation is interesting since it does not depend on detecting certain temporal features and is independent of the shape of the light curves and therefore applicable to essentially all long GRB afterglows.

In this paper, we use the same sample as Oates et al. (2012) to further explore the log L_{200s}-$\alpha_{>200\,s}$ relation observed in the optical/UV. We wish to examine whether this correlation is observed also in the X-ray and how it relates to other GRB properties. Since the observed X-ray-optical emission is predicted by the standard afterglow synchrotron model, currently the favoured scenario in terms of producing the afterglow, we will begin by predicting the relationships we should expect to observe for a sample of 48 GRBs. In this model, there is typically more than one equation to describe the relationship between two parameters. The precise equation depends on the circumstellar environment and spectral regime, which will be different for different GRBs. Therefore, we use a Monte Carlo simulation to predict the expected overall relationship for a group of GRBs with similar parameters to our sample. We also extend our analysis to include comparisons between the afterglow parameters, log $L_{200\,s}$ and $\alpha_{>200\,s}$, with prompt emission phase parameters, namely the isotropic energy E_{iso}, the peak energy E_{peak} and the duration over which 90 per cent of the prompt emission was observed T_{90}.

This paper is organized as follows. We define our sample in Sections 2 and 3 we discuss the linear regression methods we shall use throughout the paper. In Section 4, we present the analytic correlations expected from the standard afterglow model and in Section 5 we present the correlations predicted by the Monte Carlo simulation. In Section 6, we look at whether we observe these correlations within our sample of X-ray and optical/UV luminosity light curves and compare the findings with the relationships predicted by the standard afterglow model in Section 7. Finally, we conclude in Section 8. All uncertainties throughout this paper are quoted at 1σ. The temporal and spectral indices, α and β, are given by the expression $F(t, \nu) \propto t^\alpha \nu^\beta$. Throughout, we assume the Hubble parameter $H_0 = 70\,\mathrm{km\,s^{-1}\,Mpc^{-1}}$ and density parameters $\Omega_\Lambda = 0.7$ and $\Omega_m = 0.3$.

2 GRB AFTERGLOW SAMPLE

Our sample contains the same GRBs examined in Oates et al. (2012). The sample consists of 56 long duration GRBs with optical/UV afterglows, selected from the second *Swift* UVOT GRB afterglow catalogue (Roming et al., in preparation), which were observed between 2005 April and 2010 December. They were selected using the criteria of Oates et al. (2009); the optical/UV light curves must have a peak UVOT v-band magnitude of ≤17.89 (equivalent to a count rate of 1 s^{-1}), UVOT must observe within the first 400 s until at least 10^5 s after the BAT trigger and the colour of the afterglows must not evolve significantly with time, meaning that at no stage should the light curve from a single filter significantly deviate from any other filter light curve when normalized to the v filter. These criteria ensure that a high signal-to-noise (SN) light curve, covering both early and late times, could be constructed from the UVOT multifilter observations (see Oates et al. 2009, 2012, for further details). Furthermore, these GRBs have spectroscopic or photometric redshifts and we were able to determine the host $E(B − V)$ values (the host extinction was derived from spectral energy distributions (SEDs) constructed from the afterglow emission following the methodology in Schady et al. 2010). For each GRB, optical luminosity light curves were produced at a common wavelength of 1600 Å (Oates et al. 2012). This wavelength was selected to maximize the number of GRBs with SEDs that covered this wavelength and to be relatively unaffected by host extinction. A k-correction factor, k, was computed for each GRB. This was taken as the flux density at the wavelength that corresponds to 1600 Å in the rest frame, F_{1600}, divided by the flux density at the observed central wavelength of the v filter (5402 Å), F_v, which was multiplied by $(1 + z)$, where z is the redshift of the GRB such that $k = (F_{1600}/(F_v{}^*(1 + z)))$. For those GRBs with SEDs not covering 1600 Å, an average k value was determined from the other GRBs in the sample, which have SEDs covering both 1600 Å and the v filter rest-frame wavelength.

The time of each light curve was corrected to the rest frame by $t_{\mathrm{rest}} = t_{\mathrm{obs}}/(1 + z)$. The luminosity light curves were also corrected for Galactic and host extinction.

All 56 GRBs in the optical/UV sample have X-ray counterparts. The X-ray light curves were retrieved from the University of Leicester *Swift* XRT GRB data repository (Evans et al. 2007, 2009). The 0.3–10 keV flux light curves were converted to luminosity at rest-frame 1 keV. They were *k*-corrected using a *k*-correction of $(1 + z)^{-(1 + \beta)}$ (e.g. Berger, Kulkarni & Frail 2003), where the β is from spectral modelling. The time of each light curve was corrected to the rest frame by $t_{\mathrm{rest}} = t_{\mathrm{obs}}/(1 + z)$. The X-ray luminosity light curves were also corrected for Galactic and host neutral hydrogen absorption.

We selected rest frame 200 s as the time to obtain the luminosity and the time from which to fit a power law to the afterglow light curves since before this time the optical afterglows are variable and may be rising to a peak. This behaviour typically ends before rest frame 200s. Also by this time, the initial steep decay segment for the majority of X-ray light curves in our sample with this feature ceases. This steep decay segment is likely the tail of the prompt emission (Zhang et al. 2006). Therefore for each GRB, we interpolated the optical luminosity at 200 s using data between 100 and 2000 s and for the X-ray we measured the luminosity at 200 s from the best-fitting light-curve model (Racusin et al. 2009). To obtain the average decay rate, we fit a single power law to each optical and X-ray light curve using data from 200 s onwards. For eight optical/UV light curves, we were unable to determine one or both of the luminosity at 200 s and the average decay index. We therefore excluded these GRBs from our sample.

While the initial steep decay is not observed at rest frame 200 s for most of the X-ray light curves in our sample, it is present at rest frame 200 s for eight GRBs. We identify a light-curve segment to have a prompt origin if there is a steep to shallow transition with $\Delta\alpha > 1.0$. In these situations, the average decay index is measured with a simple power-law fit to data beyond rest frame 200 s and after the steep to shallow transition. In order to get a better estimate of the afterglow luminosity at rest frame 200 s, we extrapolate back to rest frame 200 s the first segment of the best-fitting light curve that is not contaminated by the prompt emission (see also Racusin et al. 2015).

We do not observe flares in the optical/UV or X-ray light curves at rest frame 200s. However, flares present after rest frame 200s may affect the observed average decay index and therefore introduce some scatter in correlations. Furthermore, the X-ray shallow decay segment may be comprised of emission from the prompt and afterglow phases. An indication of this would be evolution of the X-ray hardness ratio as the light-curve transitions from being a combination of the prompt and afterglow emission to only produced by the afterglow. We have checked the X-ray hardness ratios, from rest frame 200 s onwards, for all the X-ray afterglows in our sample and we do not find strong evidence for evolution, suggesting that the prompt emission does not strongly affect the X-ray afterglow for these GRBs. A reverse shock is also expected to be observed in the early optical/UV light curve, but is not commonly observed (Oates et al. 2009). We can assume that at rest frame 200 s, the reverse shock has either ceased or contributes at a similar or lower level as the forward shock emission for the optical/UV light curves in our sample. However, a reverse shock could also be a cause of scatter in the correlations involving parameters from the optical/UV afterglow.

In order to compare the afterglow properties with the prompt emission properties, we determined the isotropic gamma-ray energy E_{iso} and peak energy, E_{peak} from the gamma-ray emission,

following Racusin et al. (2009). The BAT fluence was converted to E_{iso} at a rest-frame bandpass of 10–10 000 keV using equation 4 from Bloom, Frail & Sari (2001). The *k*-correction was computed using the Band function (Band et al. 1993). Where available, the spectral parameters for the Band function were obtained from the 2nd *Swift* BAT catalogue (Sakamoto et al. 2011), the *Fermi* GBM catalogue (Paciesas et al. 2012) and *Konus-Wind* Gamma-ray Coordinates Network (GCN). When available, we used the measured spectral slopes, otherwise we assume $\alpha = 1$ and $\beta = 2.5$. In the cases where no E_{peak} was reported we used the correlation between the peak energy and the photon index of the νF_{ν} spectrum to estimate E_{peak} (see Sakamoto et al. 2009, for further details). The relationship can only be used to estimate E_{peak} when the power-law index of the BAT spectrum is between -2.3 and -1.3, which places E_{peak} approximately within the BAT range (see also Racusin et al. 2009, for further details). For three GRBs, E_{peak} was not reported and we were unable to use the Sakamoto relation to provide an estimate. In these cases, when calculating E_{iso} we assumed a power-law spectrum. Of the 48 GRBs in our sample, we were able to determine E_{peak} for 44 and E_{iso} for 47 GRBs. Furthermore, it is difficult to reliably determine the errors on E_{peak} and E_{iso} and so we only have error bars for a handful of them. As detailed in the next section, when performing the linear regression involving E_{peak} or E_{iso}, we did not use the FITEXY IDL regression routine, but rather SIXLIN IDL code, which does not require errors on either parameter. However, by using SIXLIN we are assuming each point has similar weighting. This may not be the case since E_{peak} is derived from two different methods. The Sakamoto relationship is an estimate of the likely E_{peak} and typically has a 1σ uncertainty in E_{peak} that is larger than the 90 per cent error found for BAT derived E_{peak} values. All the main parameters used in this paper for the correlations can be found in the appendix, see Table A1.

3 LINEAR REGRESSION

For the linear regression, we use the IDL routines FITEXY and SIXLIN: FITEXY is used when both parameters have errors, SIXLIN is used when we do not know the errors on one or both parameters. Since there are only a handful of GRBs with errors on the E_{iso} and E_{peak} parameters in order to maintain a large number of events for the regression, we choose to discard errors in both parameters. We therefore use the SIXLIN regression routine when one of the parameters involved is E_{iso}, E_{peak} or T90.

The routine SIXLIN produces the results of six linear regression methods outlined in Isobe et al. (1990). We want to determine the best physical relationship between two parameters, not the predictive relationship that results in a value of y given x, which is typically irreversible (i.e. for linear regressions $y = m_1 x + c_1$ & $x = m_2 y + c_2$, $m_1 \neq 1/m_2$ and $c_1 \neq c_2/m_2$). Of the six routines in the SIXLIN function, Isobe et al. (1990) recommend the bisector model, which is independent of the choice of x and y. This routine determines the mean slope between the ordinary least squares regression of x versus y, and y versus x. However, when there is little or no correlation between the parameters, the resulting bisector slope can be misleading,[1] if not read in conjunction with the

---

[1] For instance, if there is little correlation between two parameters, with points spread out along the x-axis, the ordinary least squares regression of x versus y would give a slope close to zero, while y versus x would give a large value. The bisector regression model would return a slope somewhere in between.

Spearman rank coefficient. This is a particular issue when performing the Monte Carlo simulation in Section 7. We therefore, report the best-fitting regression using the orthogonal regression. The orthogonal regression method is symmetric, providing a consistent result regardless of whether the regression is applied to *x* versus *y* or *y* versus *x*. This method is only recommended if the parameters involved are scale-free, i.e. logarithmic, or are scale-invariant (Isobe et al. 1990). In this paper, it is appropriate to use the orthogonal regression since the temporal decay index is scale invariant and all other parameters are ratios or are logarithms.

A final point raised by Isobe et al. (1990) and Feigelson & Babu (1992), which we address at the end of this section, is that for small samples ($N < 50$) the errors on the regression parameters may be underestimated and in this case it is more appropriate to use a bootstrap method to provide an estimate of these errors.

The routine FITEXY is based on the procedure provided by Press et al. (1992) and also has the advantage that the input variables *x* and *y* are treated symmetrically so we do not need to assume that *x* is the independent variable and *y* is the dependent variable. However, while this method takes into account measurement errors in both parameters, it does not take in to account intrinsic scatter in the data. The estimates of the errors of the slope and constant parameters are therefore typically too small and again in this case it is more appropriate to use a bootstrap method to provide an estimate to the errors on the regression parameters.

We therefore chose to determine the errors for both routines using the bootstrap method. For 10^4 trials, we randomly selected from the input data, a sample of points the same size as the input data. After one point was selected at random, we returned it to the set of observed data points, allowing it to be selected more than once during each trial. Once a set of points had been selected equal in size to the observed data set, we ran FITEXY or SIXLIN on this set of points. For each of the 10^4 trials, we recorded the slope and constant value. To provide the 1σ errors, we separately ordered the recorded sets of slope and constant values by size and selected the upper and lower errors as the difference between the mean and the values at 15.9 and 84.1 per cent. During this process, a Spearman rank correlation was also performed on the simulated data so that we could obtain the 1σ errors given in Table 2 in a similar fashion.

4 THE STANDARD SYNCHROTRON AFTERGLOW MODEL

The standard afterglow synchrotron model is currently the favoured scenario in terms of producing the observed X-ray-optical afterglow emission. In this model, the afterglow is a natural result of the collimated ejecta reaching the external medium and interacting with it, producing the observed synchrotron emission. For a given frequency, the observed flux depends on the position of the frequency relative to the synchrotron frequencies (the synchrotron cooling frequency ν_c, the synchrotron peak frequency ν_m and the synchrotron self-absorption frequency ν_a) and the values of the microphysical parameters (the kinetic energy of the outflow E_k, the fraction of energy given to the electrons ϵ_e, the fraction of energy given to the magnetic field ϵ_B, the structure and density of the external medium and the electron energy index *p*). Therefore, it is possible to predict the relationships between observable and/or microphysical parameters at any time during the afterglow (e.g. Sari, Piran & Narayan 1998; Panaitescu & Kumar 2000; Gao et al. 2013). Since the kinetic energy E_k and the isotropic energy E_{iso} are related linearly through the efficiency parameter $\eta = E_{iso}/(E_{iso} + E_k)$ and the luminosity

is a function of E_k, we can also predict the relationship between optical/UV and X-ray luminosities and E_{iso}.

We now derive the relationships we should expect in our observed sample of optical/UV and X-ray luminosity light curves. We use the expectations for flux in (Sari et al. 1998, , see their equation 8) and the equations for peak flux, $F_{\nu,max}$, ν_c and ν_m in Zhang et al. (2007). We assume an isotropic, collimated outflow which is not energy injected and since we wish to consider a very simplistic model we do not consider the emission from the traditional reverse shock (e.g. Zhang, Kobayashi & Mészáros 2003). We can justify excluding the contribution from the reverse shock because we only examine parameters at or beyond rest frame 200 s, by which time the reverse shock in most cases has either ceased or contributes at a similar or lower level to the forward shock emission (e.g. Oates et al. 2007).

Studies of individual GRBs and samples of GRBs suggest that a large fraction of afterglows are produced by outflows ploughing into constant density media (e.g. Oates et al. 2009; Rykoff et al. 2009; Schulze et al. 2011). Therefore, we shall only consider relationships appropriate for this density medium. This assumption will be verified later in Section 7. As the optical/UV and X-ray emission is likely to be above ν_m at rest frame 200 s, we also only consider the most likely spectral regimes either $\nu_m < \nu_O < \nu_c < \nu_X$, $\nu_m < \nu_O < \nu_X < \nu_c$ or $\nu_m < \nu_c < \nu_O < \nu_X$.

Under these conditions there are three possible relationships between optical and X-ray luminosity in the standard afterglow model,

$$L_X = \begin{cases} \left(\frac{\nu_X}{\nu_O}\right)^{-(p-1)/2} L_O & : \nu_m < \nu_O < \nu_X < \nu_c \\ \left(\frac{\nu_X}{\nu_c}\right)^{p/2}\left(\frac{\nu_O}{\nu_c}\right)^{-1/2} L_O & : \nu_m < \nu_O < \nu_c < \nu_X \\ \left(\frac{\nu_X}{\nu_O}\right)^{-p/2} L_O & : \nu_m < \nu_c < \nu_O < \nu_X, \end{cases} \quad (1)$$

where *p* is the energy distribution index ($dN(E)/dE \propto E^p$; where $N(E)$ is the number of electrons with energy, E). Each scenario predicts a linear relationship, with a normalization that is dependent on *p*, and for the second regime only, also dependent on the value of ν_c. These relationships suggest that for a distribution of L_X versus L_O, we may expect to observe two different lines, corresponding to the first and third relationships of equation (1), bridged together by data points corresponding to the $\nu_m < \nu_O < \nu_c < \nu_X$ relationship.

The standard afterglow model also predicts relationships between L_ν, at a given frequency ν, with kinetic energy E_k as

$$L_\nu \propto \begin{cases} E_k^{\left(\frac{p+3}{4}\right)} & : \nu_m < \nu < \nu_c \\ E_k^{\left(\frac{p+2}{4}\right)} & : \nu_m < \nu_c < \nu. \end{cases} \quad (2)$$

Predicting the observed relationship is complicated by the fact that we need to know the value for the efficiency in order to get the direct relationship between $L_{200\,s}$ and E_{iso}.

Finally, we can easily show what we should expect, in terms of the standard afterglow model, for the relationship of (L_O/L_X) with energy,

$$\frac{L_O}{L_X} = \begin{cases} \left(\frac{\nu_O}{\nu_X}\right)^{-(p-1)/2} & : \nu_m < \nu_O < \nu_X < \nu_c \\ \left(\frac{\nu_O}{\nu_X}\right)^{-p/2}\left(\frac{\nu_O}{\nu_c}\right)^{1/2} \propto E_k^{1/4} & : \nu_m < \nu_O < \nu_c < \nu_X \\ \left(\frac{\nu_O}{\nu_X}\right)^{-p/2} & : \nu_m < \nu_c < \nu_O < \nu_X. \end{cases} \quad (3)$$

When the optical/UV and X-ray bands lie on the same segment, $\log (L_O/L_X)$ is independent of $\log E_{iso}$, but is dependent on *p*. Assuming a range for *p* of between 2.0 and 3.0, this ratio of the

optical/UV and X-ray luminosities lies between 1.05 and 3.16 (where $\nu_O = 1.87 \times 10^{15}$ Hz and $\nu_X = 2.4 \times 10^{17}$ Hz). When the X-ray and optical/UV bands lie on different segments, the ratio will range between 1.05 and 3.16, but the ratio is dependent on the choice of energy, such that the ratio increases with $E_k^{1/4}$.

In equations (1), (2) and (3), there are several possibilities for how the parameters are related and it is likely that different GRBs are in different regimes and so satisfy different formulae. This makes a simple analytic prediction of the expected relationships in a sample of observed parameters difficult to determine. Therefore in Section 5, we use a Monte Carlo simulation to predict the correlations we should actually observe, between these and other parameters, when using a sample of GRB afterglows.

5 MONTE CARLO SIMULATION

Since the standard afterglow model does not offer a single equation for the relationships between parameters, we employed the use of a Monte Carlo simulation, to determine what relationships we should expect from this model with the same number of GRBs as our sample. Using 10^4 trials, we simulated the optical/UV (at 1600 Å) and X-ray (at 1 keV) flux densities for 48 GRBs using equation 8 of Sari et al. (1998) and equations 4, 5 and 6 given in Zhang et al. (2007) for $F_{\nu,\max}$, ν_m and ν_c. In this simulation, we assume that all GRBs are produced in a constant density medium, consistent with our assumption detailed in Section 4. To compute $F_{\nu,\max}$, ν_m and ν_c, we needed to provide values for the microphysical parameters. These were selected at random from lognormal distributions which had 3σ intervals ranging between 0.01 and 0.3 for the fraction of energy given to the electrons, ϵ_e; 5×10^{-4}–0.5 for the fraction of energy given to the magnetic field, ϵ_B, and 10^{-3}–$10^3 \mathrm{cm}^{-2}$ for the density of the external medium. The centre of each of these distributions is at the logarithmic mid-point. For the electron energy index p, we centred the distribution at 2.4, as determined by Curran et al. (2009), however, we set the 1σ width to be 0.2 rather than 0.59. Since the closure relations fail for p values <2, we re-sampled the p value when $p < 2$ was selected. The value of p along with the position of ν_c relative to the observed band and redshift (selected from a uniform distribution with the range 0.5–4.5, a similar range as the observed sample), dictate the values of α, β and the k-correction (as given in Berger et al. 2003).

For the 48 GRBs in each trial, we selected a prompt emission energy from a lognormal distribution with a 3σ range 10^{51}–10^{54} erg. This range and distribution was selected to be similar to that of the GRBs in this paper, e.g. Table A1. We picked a random value between 10 and 99 per cent for the efficiency, which we used to convert the prompt emission energy into kinetic energy. Once all the microphysical parameters, redshift and kinetic energy had been selected, we were then able to determine the position of ν_c and thus knew where it was in relation to ν_O and ν_X. With this information, we then calculated the value of the optical and X-ray fluxes and converted these to luminosity; a k-correction was applied during this conversion. We finally took the logarithm of both parameters. As a byproduct of calculating the optical and X-ray luminosities, we also have simulated distributions for E_{iso} and α. Therefore, we also produce predictions for comparisons that involve these parameters in addition to those examined in Section 4.

Once a sample of 48 GRBs had been constructed, we then performed linear regressions, using the IDL routine SIXLIN, and we also calculated the Spearman rank coefficient. We repeated the above until we completed all 10^4 trials. From this routine, we obtained the best-fitting slopes to the correlations between several parameters:

the optical/UV and X-ray luminosities, the optical/UV and X-ray decay indices and E_{iso}. The pairs of parameters can be found in Table 1. For each distribution of slope values, we take the mean and the 1σ error to be the difference between the mean and the 15.9 and 84.1 per cent values (when the data are ordered numerically).

6 OBSERVATIONAL RESULTS

In this section, we now determine what correlations we find in the observed sample of 48 GRB afterglows. We use the Spearman rank correlation to determine if two parameters are correlated and linear regression to quantify the degree of correlation and the relationship between these parameters. The results of the Spearman rank tests and linear regressions for all correlations can be found in Table 2. In this table, we also include the partial Spearman rank correlation, which measures the degree of correlation between two parameters, excluding the effect of a third, in this case redshift (see Kendall & Stuart 1979, for further details).

In Oates et al. (2012), a correlation was discovered between the logarithmic luminosity at 200 s and the average decay rate of optical/UV light curves, measured from 200 s onwards. We now examine if a similar relationship is observed in the X-ray light curves. The best fits to the linear regressions for these correlations: $\log L_{X,200\,s} - \alpha_{X,>200\,s}$ and $\log L_{O,200\,s} - \alpha_{O,>200\,s}$ can be found in Table 2. Similar to that found in the optical/UV, we find a significant relationship between the luminosity and decay rate of the X-ray light curves (see also Racusin et al. 2015). For the two frequencies, we find the linear regression gives relationships that are consistent at 1σ.

The X-ray light curves in our sample display a wide range in behaviour, ranging from X-ray light curves with simple power-law decay to GRBs with 4–5 breaks. Since Dainotti et al. (2008) have shown a correlation between the luminosity at the end of the X-ray plateau with the time the plateau phase ceases, we examined whether the plateau phase plays a role in our correlation. In our sample, we find 35 GRBs that have a plateau following the criteria of Racusin et al. (2009). Repeating the Spearman rank correlation for $\log L_{X,200\,s}-\alpha_{X,>200\,s}$ for these GRBs, we find a coefficient of -0.73 at a confidence of 4.97σ, indicating a strong correlation. For the 13 GRBs without X-ray plateau phase, repeating the Spearman rank correlation, we find a coefficient of -0.32 at 72 per cent confidence. It is inconclusive whether or not there is a correlation between $\log L_{X,200\,s}-\alpha_{X,>200\,s}$ for the GRBs without X-ray plateau phase. However considering for the full sample of GRBs, the X-ray and optical/UV light curves have consistent linear regressions (the optical light curves do not typically have a well-defined plateau phase), suggests that the correlation does not depend on having a plateau phase in the optical or X-ray light curves. This is also supported by the results of a similar comparison using a larger X-ray sample (Racusin et al. 2015). Therefore, in this paper we do not distinguish further between GRBs with and without X-ray plateaus.

Since equation (1) predicts a relationship between luminosity of the X-ray and optical/UV afterglows and we find correlations that show that intrinsically the brightest afterglows decay the quickest, we now examine and compare the $\log L_{200\,s}$ and $\alpha_{>200\,s}$ parameters of the optical/UV and X-ray light curves.

6.1 Afterglow parameter comparison

In the top panel of Fig. 1, we compare the optical/UV and X-ray luminosities at 200 s, $\log L_{O,200\,s}$ and $\log L_{X,200\,s}$, respectively.

Table 1. The Spearman rank coefficient and linear regression parameters as predicted by the synchrotron model for a sample of 48 GRBs. These values were computed with a Monte Carlo simulation with 10^4 trials.

Parameters		Simulated Spearman	Best-fitting linear regression for simulation	
x-axis	y-axis	Rank coefficient	Slope	Constant
$\log L_{O,200s}$	$\log L_{X,200s}$	0.92 ± 0.02	0.82 ± 0.04	3.76 ± 1.25
$\alpha_{O,>200s}$	$\alpha_{X,>200s}$	0.74 ± 0.06	1.10 ± 0.15	-0.04 ± 0.17
$\log L_{O,200s}$	$\alpha_{O,>200s}$	-0.30 ± 0.14	-0.04 ± 0.02	0.31 ± 0.65
$\log L_{X,200s}$	$\alpha_{X,>200s}$	-0.20 ± 0.14	-0.04 ± 0.03	-0.10 ± 0.78
$\log E_{iso}$	$\alpha_{O,>200s}$	-0.06 ± 0.15	-0.03 ± 0.06	0.32 ± 2.91
$\log E_{iso}$	$\alpha_{X,>200s}$	-0.09 ± 0.15	-0.04 ± 0.06	0.76 ± 3.13
$\log E_{iso}$	$\log L_{O,200s}$	0.51 ± 0.11	4.43 ± 1.03	-200.76 ± 54.10
$\log E_{iso}$	$\log L_{X,200s}$	0.54 ± 0.11	3.28 ± 0.71	-142.22 ± 37.33

Table 2. For each pair of parameters examined, this table provides: the Spearman rank correlation coefficient with its associated null hypothesis; the coefficient of the partial Spearman rank with its associated null hypothesis, which tests the correlation between two parameters taking into account the parameters dependence on redshift; the slope and constant values provided by the best-fitting linear regression. For comparison with our Monte Carlo simulations in Section 7, we also provide the 1σ error of the Spearman rank coefficient.

Parameters		Spearman rank	Null	Partial	Null	Best-fitting linear regression	
x-axis	y-axis	coefficient	hypothesis	Spearman rank	hypothesis	Slope	Constant
$\log L_{O,200s}$	$\log L_{X,200s}$	$0.81\,(0.05)$	5.26×10^{-12}	0.70	2.85×10^{-8}	0.91 ± 0.22	1.04 ± 6.82
$\alpha_{O,>200s}$	$\alpha_{X,>200s}$	$0.77\,(0.07)$	1.10×10^{-10}	0.75	1.27×10^{-9}	0.97 ± 0.10	-0.25 ± 0.09
$\log L_{O,200s}$	$\alpha_{O,>200s}$	$-0.58\,(0.11)$	1.90×10^{-5}	-0.50	2.85×10^{-4}	-0.28 ± 0.04	7.72 ± 1.31
$\log L_{X,200s}$	$\alpha_{X,>200s}$	$-0.69\,(0.09)$	8.03×10^{-8}	-0.63	1.58×10^{-6}	-0.26 ± 0.05	6.71 ± 1.39
$\log L_{O,200s}$	$\alpha_{X,>200s}$	$-0.60\,(0.12)$	6.87×10^{-6}	-0.52	1.53×10^{-4}	-0.29 ± 0.03	8.13 ± 1.08
$\log L_{X,200s}$	$\alpha_{O,>200s}$	$-0.65\,(0.10)$	5.58×10^{-7}	-0.60	7.58×10^{-6}	-0.32 ± 0.06	8.70 ± 1.68
$\log E_{iso}$	$\alpha_{O,>200s}$	$-0.54\,(0.12)$	9.05×10^{-5}	-0.44	1.96×10^{-3}	-0.21 ± 0.05	10.22 ± 2.57
$\log E_{iso}$	$\alpha_{X,>200s}$	$-0.57\,(0.11)$	3.12×10^{-5}	-0.47	8.70×10^{-4}	-0.21 ± 0.04	9.60 ± 2.16
$\log E_{iso}$	$\log L_{O,200s}$	$0.76\,(0.06)$	4.51×10^{-10}	0.66	4.59×10^{-7}	1.09 ± 0.13	-25.27 ± 6.92
$\log E_{iso}$	$\log L_{X,200s}$	$0.83\,(0.05)$	5.04×10^{-13}	0.76	4.78×10^{-10}	1.10 ± 0.15	-27.81 ± 7.89
$\log E_{iso}$	$\log (L_{O,200s}/L_{X,200s})$	$-0.06\,(0.16)$	7.10×10^{-1}	-0.14	3.56×10^{-1}	-0.10 ± 0.19	7.54 ± 9.82
$\log E_{peak}$	$\alpha_{O,>200s}$	$-0.45\,(0.13)$	2.05×10^{-3}	-0.38	1.20×10^{-2}	-0.48 ± 0.17	0.22 ± 0.41
$\log E_{peak}$	$\alpha_{X,>200s}$	$-0.48\,(0.13)$	9.22×10^{-4}	-0.40	7.52×10^{-3}	-0.48 ± 0.15	-0.03 ± 0.36
$\log E_{peak}$	$\log L_{O,200s}$	$0.66\,(0.11)$	1.16×10^{-6}	0.58	3.51×10^{-5}	2.97 ± 0.76	24.53 ± 1.95
$\log E_{peak}$	$\log L_{X,200s}$	$0.75\,(0.10)$	4.74×10^{-9}	0.70	1.38×10^{-7}	2.97 ± 0.67	22.50 ± 1.73
$\log T90_{rest}$	$\alpha_{O,>200s}$	$-0.23\,(0.14)$	1.15×10^{-1}	-0.21	1.61×10^{-1}	-0.19 ± 0.10	-0.75 ± 0.12
$\log T90_{rest}$	$\alpha_{X,>200s}$	$-0.13\,(0.14)$	3.71×10^{-1}	-0.10	5.03×10^{-1}	-0.12 ± 0.09	-1.08 ± 0.11
$\log T90_{rest}$	$\log L_{O,200s}$	$0.26\,(0.14)$	7.58×10^{-2}	0.24	9.85×10^{-2}	4.41 ± 2.59	26.28 ± 3.49
$\log T90_{rest}$	$\log L_{X,200s}$	$0.14\,(0.15)$	3.58×10^{-1}	0.09	5.58×10^{-1}	10.60 ± 12.99	16.35 ± 16.70
$\log T90_{rest}$	$\log E_{iso}$	$0.43\,(0.12)$	2.65×10^{-3}	0.43	2.34×10^{-3}	2.30 ± 0.57	49.70 ± 0.80
$\log T90_{rest}$	$\log E_{peak}$	$0.23\,(0.16)$	1.26×10^{-1}	0.21	1.69×10^{-1}	0.46 ± 0.21	1.90 ± 0.25

There is a strong positive correlation between the luminosity in the X-ray and optical/UV bands at 200 s, which is confirmed by a Spearman rank correlation coefficient of 0.81 at a significance of 6.9σ. A linear regression of the two parameters results in a relationship close to unity, with the slope 0.91 ± 0.22.

In the bottom panel of Fig. 1, we compare the average decay rate determined from 200 s onwards of the optical/UV and X-ray light curves, $\alpha_{O,>200s}$ and $\alpha_{X,>200s}$, respectively. Spearman rank gives a correlation coefficient of 0.77 at a significance of 6.5σ.

In Table 2, we also provide the relationships derived when swapping the X-ray and optical luminosity decay parameters, i.e. $\log L_{O,200s}$ versus $\alpha_{X,>200s}$ and $\log L_{X,200s}$ versus $\alpha_{O,>200s}$. The fact that significant correlations are found even when mixing decay and luminosity parameters between the optical/UV and X-ray bands provides support to the correlations discussed in this section.

6.2 Prompt emission and afterglow parameter comparison

In the following, we examine the relationship between $\log L_{200s}$ and $\alpha_{>200s}$ with $\log E_{iso}$ for both the optical/UV and X-ray light curves, so that we may compare the observed correlations with our simulations. We will also compare the afterglow parameters with other basic properties of the prompt emission.

6.2.1 Prompt emission: isotropic energy

Comparisons between afterglow luminosity and isotropic energy have been previously reported. Early reports showed that the luminosity at 12 h to 1 d after the trigger correlates well with the isotropic gamma-ray energy (e.g. Kouveliotou et al. 2004; De Pasquale et al. 2006; Nysewander, Fruchter & Pe'er 2009; Kann et al. 2010). More recently D'Avanzo et al. (2012) and Margutti et al. (2013), showed that in the X-rays, measurements of the luminosity during the early afterglow, approximately 5–10 min after trigger, have less scatter and the correlations are stronger in comparison with measurements taken at any subsequent time later. We may also thus expect this to be the case in the optical. In the top two panels of Fig. 2, we display the logarithmic isotropic gamma-ray energy, $\log E_{iso}$ against $\log L_{O,200s}$ and $\log L_{X,200s}$. Spearman rank correlations of the luminosity parameters against $\log E_{iso}$ provide correlation
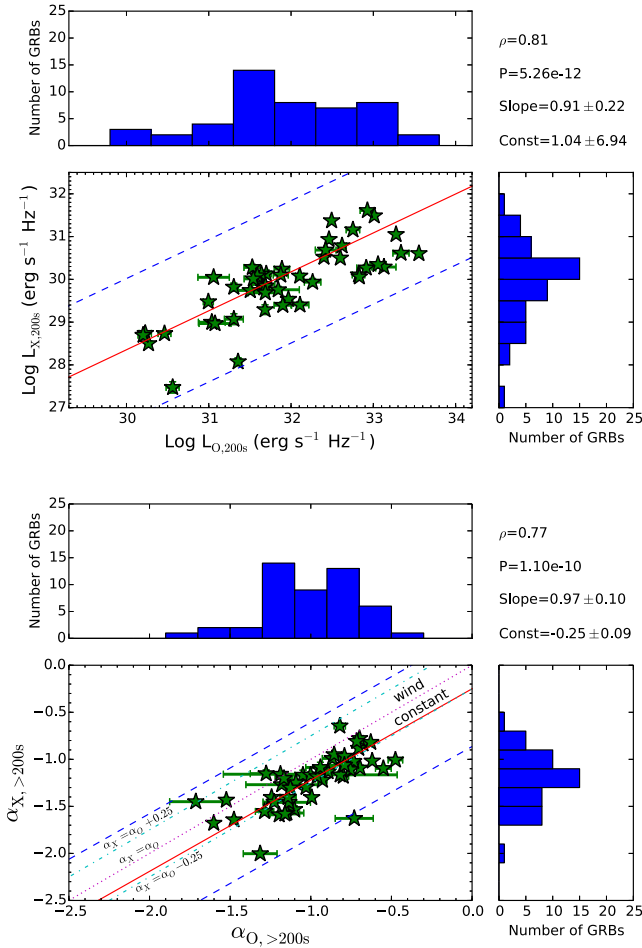
Figure 1. Top: optical/UV and X-ray luminosity determined at rest frame 200 s. Bottom: average decay rate of the optical/UV and X-ray light curves determined from rest frame 200 s onwards. In both panels, the red solid line represents the best-fitting regression and the blue dashed line represents three times the root mean square (RMS) deviation. In the bottom panel, we also show relationships expected between the optical/UV and X-ray light curves from the GRB closure relations. The pink dotted line represents the optical/UV and X-ray decay indices being equal. The light blue dot–dashed lines represent the X-ray temporal index equal to the optical/UV temporal index $\pm$ 0.25. In the top-right corner of each panel, we give the Spearman rank coefficient, ρ, and corresponding null hypothesis probability, P, and we provide the best-fitting slope and constant determined by linear regression.

coefficients of 0.76 and 0.83 with significances of 6.2σ and 7.2σ for the optical/UV and X-ray afterglows, respectively. In comparison to Nysewander et al. (2009) and Kann et al. (2010), who compare the optical/UV luminosity with E_{iso} at 11 h and 1 d, respectively, we see less spread using the luminosity at earlier times, as expected in comparison to the X-ray light curves. For both the optical/UV and X-ray light curves, the linear regressions of the log $L_{200\,s}$ and log E_{iso}, give consistent results within 1σ errors.

In Fig. 3, we display the relationship between log $L_{O,200\,s}$ and log $L_{X,200\,s}$ with log E_{iso}, as the logarithm of the ratio between the optical/UV and X-ray luminosities against log E_{iso} (see equation 3). There is no evidence for correlation between these parameters.

In the bottom two panels of Fig. 2, we display log E_{iso} against $\alpha_{O,>200\,s}$ and $\alpha_{X,>200\,s}$. Both panels indicate correlations between the average decay indices with isotropic energy. This suggests that the more energetic the prompt emission, the faster the average decay of

the X-ray and optical/UV afterglows. Spearman rank correlations of the average decay parameters against log E_{iso} provide correlation coefficients of -0.54 and -0.57 for the optical/UV and X-ray afterglows, at confidences of 3.9σ and 4.2σ, respectively. These correlations are slightly less strong in comparison to that found between the luminosity and log E_{iso}. We note that within errors the equations for the linear regression for both the optical/UV and X-ray decay indices against log E_{iso} are consistent with each other.

6.2.2 Prompt emission: peak spectral energy

The Amati relation indicates a relationship between the isotropic gamma-ray energy E_{iso} and the rest-frame gamma-ray peak energy E_{peak} (Amati et al. 2002). Therefore, we may already predict correlations between E_{peak} and the afterglow parameters, but for completeness and to report the strength of these correlations we now briefly compare the afterglow parameters with E_{peak}.

In the top panels of Fig. 4, we display the logarithmic rest-frame peak gamma-ray energy, log E_{peak} against log $L_{O,200\,s}$ and log $L_{X,200\,s}$. Spearman rank correlations of the luminosity parameters against log E_{peak} provide evidence for correlation with coefficients of 0.75 and 0.66 for the X-ray and optical/UV light curves, respectively, with corresponding significances of 5.9σ and 4.9σ. This is consistent with D'Avanzo et al. (2012) who also show that the early X-ray luminosity (at rest frame 5 min) and log E_{peak} are correlated. We notice that the Spearman rank coefficient for the log $L_{200\,s}$ versus log E_{peak} is smaller than that found for log $L_{200\,s}$ with log E_{iso}, indicating that the relationships involving the prompt emission peak energy are weaker in comparison to the relationships observed with the isotropic energy. This is also consistent with D'Avanzo et al. (2012) who find that the correlations between the X-ray luminosity and log E_{peak} have smaller correlation coefficients than the correlation between X-ray luminosity and log E_{iso}.

The bottom panels of Fig. 4, display log E_{peak} against $\alpha_{O,>200\,s}$ and $\alpha_{X,>200\,s}$. For these correlations, the Spearman rank coefficients are smaller in comparison to the Spearman rank coefficients found for the correlations between the decay indices and log E_{iso}. The correlation of the decay indices with log E_{peak} results in coefficients of -0.45 and -0.48 for the optical/UV and X-ray afterglows, respectively, with corresponding significances of 3.1σ and 3.3σ.

6.2.3 Prompt emission: rest-frame T90 duration

In Table 2 and Fig. 5, we also provide results of the Spearman rank correlation for the duration of the gamma-ray emission in the rest frame, T90/(1 + z), with the optical/UV and X-ray log $L_{200\,s}$ and $\alpha_{>200\,s}$ parameters. Significant correlations are not found amongst these parameters. This is consistent with Margutti et al. (2013) who do not find any evidence for correlations amongst several X-ray parameters with rest frame T90.

6.3 Effect of prompt emission contaminating afterglow light curves at rest frame 200s

In order to ensure that the relationships provided in this paper are not affected by our estimation of log $L_{X,200\,s}$ and $\alpha_{X,>200\,s}$ for the GRBs whose X-ray light curves at 200 s are contaminated by the prompt emission, we exclude these eight GRBs and repeat the analysis for all pairs of parameters. We find that the results do not significantly change for correlations involving all but the rest frame T90 parameters. In these cases, we find that correlations of the different
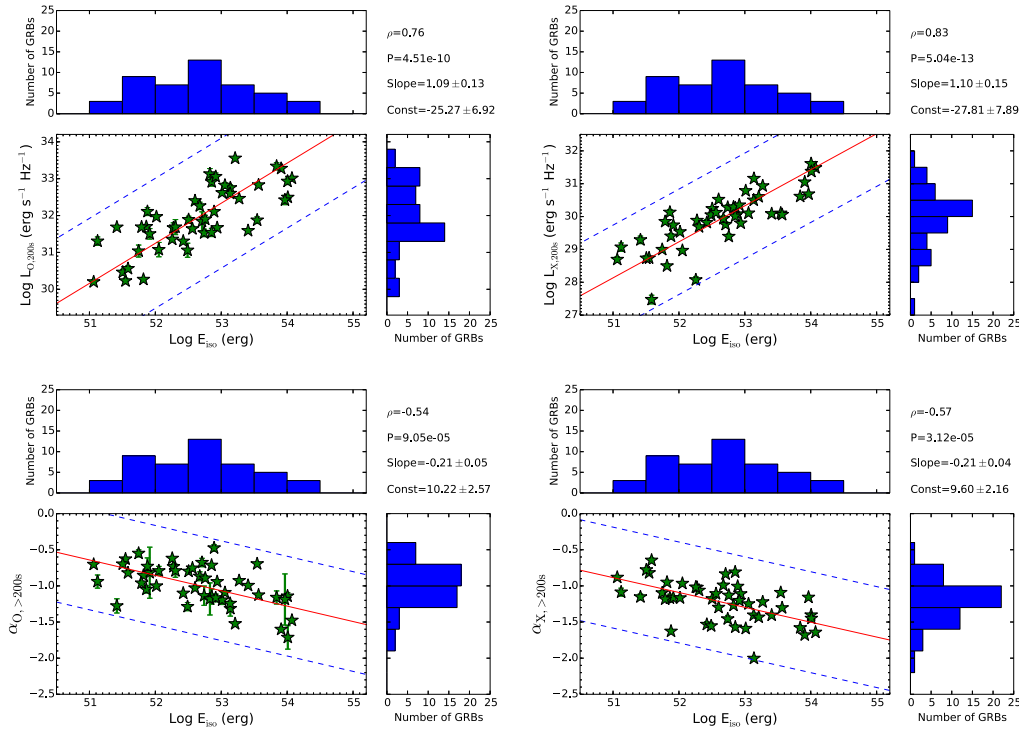
Figure 2. Top-left: the optical luminosity at rest frame 200 s versus isotropic energy. Top-right: the X-ray luminosity at rest frame 200 s versus isotropic energy. Bottom Left: the optical average decay index determined from rest frame 200 s versus isotropic energy. Bottom-right: the X-ray average decay index determined from rest frame 200 s versus isotropic energy. In all panels, the red solid line represents the best-fitting regression and the blue dashed line represents the 3σ deviation. In the top-right corner of each panel, we give the Spearman rank coefficient, ρ, and corresponding null hypothesis probability, P, and we provide the best-fitting slope and constant determined by linear regression.

parameters with rest frame T90 provide Spearman rank coefficients larger than those determined with the same analysis performed on the entire GRB sample. For most pairs of parameters, the significance implied by the Spearman rank coefficient is $<3\sigma$. For three pairs of parameters: rest frame T90 and log $L_{O,200\,s}$, rest frame T90 and log E_{iso}, and rest frame T90 with log E_{peak}, the significance of correlation implied by the Spearman rank coefficient is $>3\sigma$ and the coefficient suggests strong correlations. However, this is most likely a selection effect. In order to observe the tail of the prompt emission at rest frame 200 s, the duration of the prompt emission should be long, but also the tail of the prompt emission has to be bright enough or the afterglow weak enough so that the emission can be observed above the afterglow. For these eight GRBs, it is the chance combination of low afterglow luminosity and long duration prompt emission, which allows the tail of the prompt emission to dominate over the afterglow. It is therefore not a surprise that these light curves cluster at large rest frame T90 and low log $L_{X,200\,s}$. Also since log $L_{X,200\,s}$ correlates with log $L_{O,200\,s}$ and log E_{iso}, we should also find clustering when investigating these parameters with rest frame T90. Examining the corresponding panels of Fig. 5, we find that the eight GRBs are clustered in the bottom right of these panels. Therefore by removing these GRBs and repeating the correlations, we are artificially inducing correlations between these parameters.

7 DISCUSSION

We have explored the rest-frame properties of a sample of 48 X-ray and optical/UV afterglow light curves. We have shown that the log $L_{200\,s}$-$\alpha_{>200\,s}$ correlation observed in Oates et al. (2012) is also
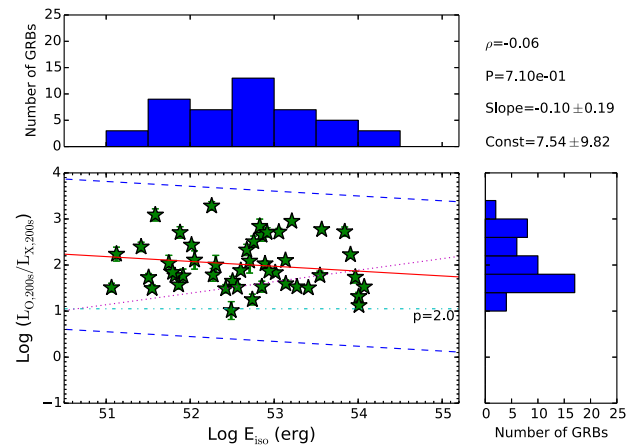

Figure 3. The ratio of the optical/UV to X-ray luminosities at 200 s versus the isotropic prompt emission E_{iso}. The red solid line represents the best-fitting regression and the blue dashed line represents the 3σ deviation. The dotted pink line represents how the ratio scales with energy in the regime $\nu_m < \nu_O < \nu_c < \nu_X$ as given in the second line of equation (3); the line has arbitrary normalization. The dot–dashed light blue line, indicates the minimum ratio value predicted from equation (3) when p is 2.0. In the top-right corner, we give the Spearman rank coefficient, ρ, and corresponding null hypothesis probability, P, and we provide the best-fitting slope and constant determined by linear regression.

observed in the X-ray light curves. It has been previous suggested that the brightest X-ray afterglows decay more quickly than fainter afterglows (Boër & Gendre 2000; Kouveliotou et al. 2004; Gendre & Boër 2005), which was based predominantly on pre-*Swift*
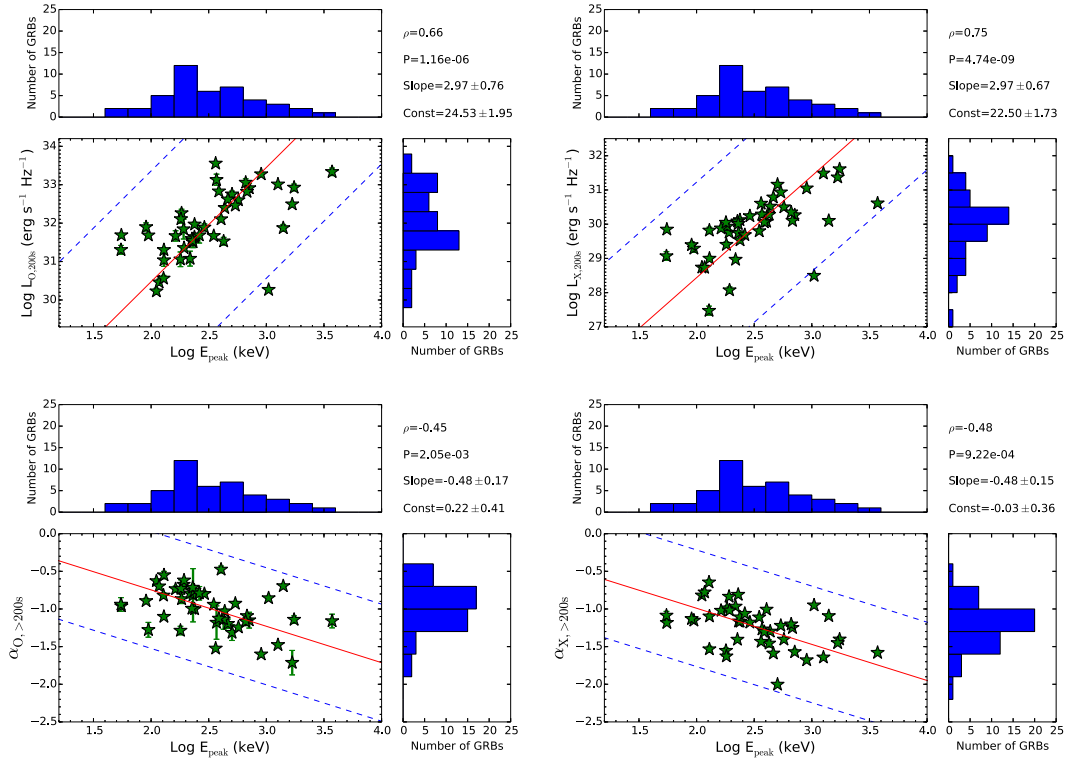
Figure 4. Top left: the optical luminosity at rest frame 200 s versus gamma-ray peak energy. Top right: the X-ray luminosity at rest frame 200 s versus gamma-ray peak energy. Bottom left: the optical average decay index determined from rest frame 200 s versus gamma-ray peak energy. Bottom right: the X-ray average decay index determined from rest frame 200 s versus gamma-ray peak energy. In all panels, the red solid line represents the best-fitting regression and the blue dashed line represents the 3σ deviation. In the top-right corner of each panel, we give the Spearman rank coefficient, ρ, and corresponding null hypothesis probability, P, and we provide the best-fitting slope and constant determined by linear regression.

observations of late-time X-ray afterglows. However, a larger sample including some of the first *Swift* X-ray light curves (Gendre et al. 2008) was not able to support previous claims (see also Racusin et al. 2015). In this paper, the correlation between X-ray luminosity and temporal behaviour examines the light curves from a much earlier time, when there is greater spread in the luminosity distribution, and the average decay index is determined using almost the entire observed afterglow. Since both the optical/UV and X-ray light curves show log $L_{200\,s}$-$\alpha_{>200\,s}$ correlations, which are consistent, this points towards a common underlying mechanism producing both the X-ray and optical afterglows. We can therefore generally exclude models that invoke different emission mechanisms that separately produce the X-ray and optical/UV afterglow.

We also have shown that the X-ray and optical/UV log $L_{200\,s}$ are correlated with log E_{iso} and E_{peak}. This is consistent with previous studies (e.g. Kouveliotou et al. 2004; De Pasquale et al. 2006; Nysewander et al. 2009; Kann et al. 2010), particularly with D'Avanzo et al. (2012) and Margutti et al. (2013), who performed a similar study using early X-ray luminosity, approximately 5–10 min after trigger. We have shown for the first time a correlation which relates the average temporal behaviour with log E_{iso} and E_{peak}. Combined with the other correlations reported in this paper, this indicates that the GRBs with the brightest, fastest, decaying afterglows also have the largest observed prompt emission energies and typically larger peak spectral energy.

We now investigate if these observations are consistent with the predictions of the standard synchrotron model in its most simple form by comparing our observations with the analytical relationships predicted in Section 4 and with the Monte Carlo simula-

tions described in Section 5. We first verify that the basic properties of our simulation are consistent with basic properties of the GRB sample. We find the simulation produces the following average values: log $L_{O,200\,s} = 32.04 \pm 1.26$, log $L_{X,200\,s} = 30.15 \pm 1.02$, $\alpha_{O,>200\,s} = -1.09 \pm 0.17$, $\alpha_{X,>200\,s} = -1.25 \pm 0.18$. These values are consistent at 1σ with the weighted averages from our sample: log $L_{O,200\,s} = 32.11 \pm 0.72$, log $L_{X,200\,s} = 30.46 \pm 0.70$, $\alpha_{O,>200\,s} = -0.97 \pm 0.07$, $\alpha_{X,>200\,s} = -1.22 \pm 0.08$. Since for the majority of GRBs in our sample, the X-ray and optical/UV light curves are consistent with lying in different parts of the spectrum, we have checked that the peak of the distribution of the synchrotron cooling frequency is consistent with lying in between the optical and X-ray bands. In this case, we obtain an average log frequency of 16.55 ± 1.19. The simulated samples are therefore consistent with being drawn from the same population as our observed data. This suggests that our initial starting parameters and assumptions were appropriate and therefore we shall continue to compare the results of the simulation in Table 1 with the observed data in Table 2.

7.1 Comparison of observed and predicted correlations

The standard afterglow model predicts several relationships between $L_{X,200\,s}$ and $L_{O,200\,s}$. Depending on the spectral regime a GRB may satisfy one of three relationships; see equation (1). In our observed sample, see Fig. 1, we are only able to observe one overall clustering of points that when fitted with a linear function produces a relationship different to those predicted in equation (1). This is not surprising since the number of GRBs in our sample is relatively small and the relationships are fairly similar. It is therefore
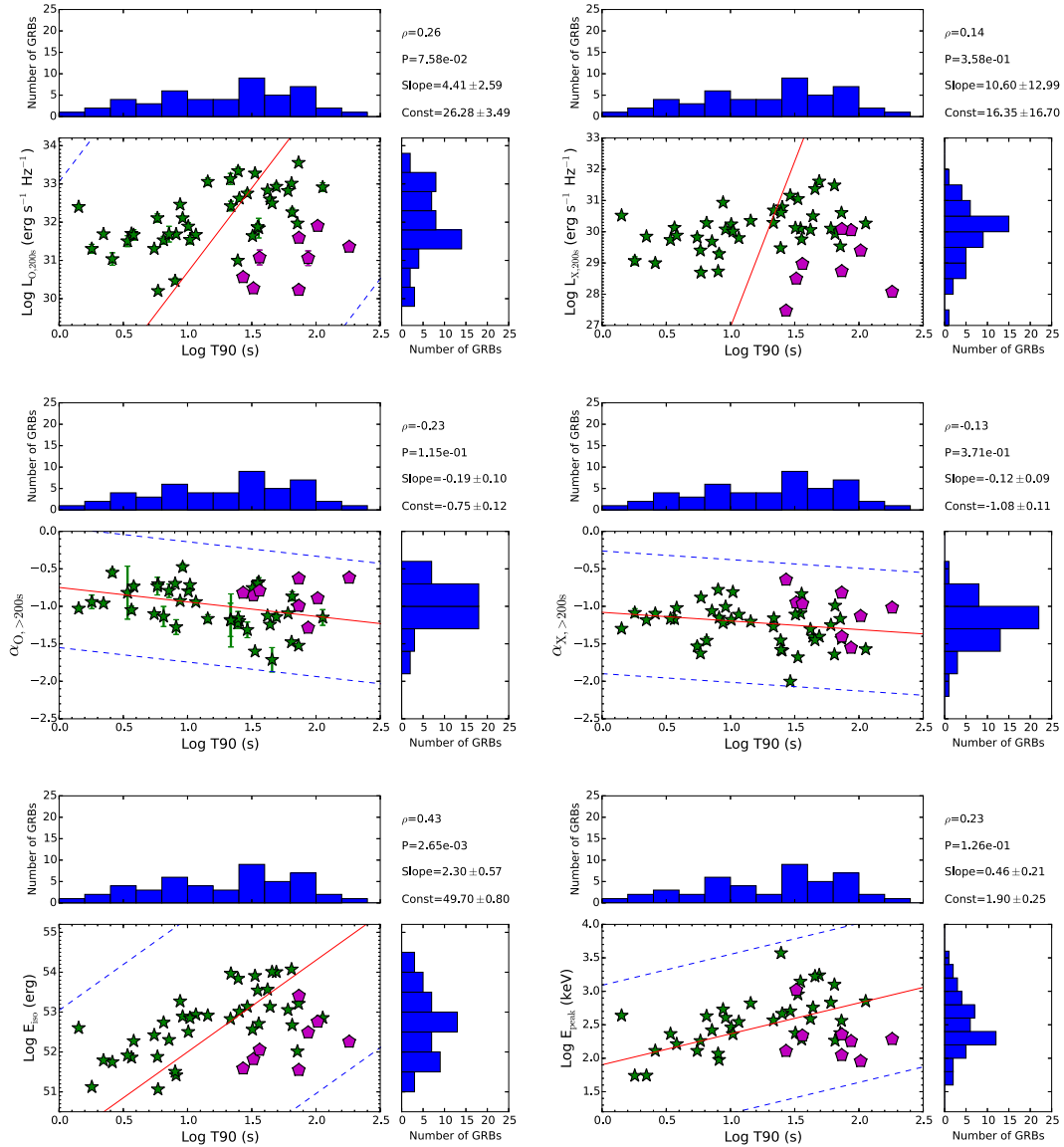
Figure 5. In this figure, we compare the rest-frame T90 parameter with the luminosity and average decay slopes of the optical/UV and X-ray light curves, and also the isotropic energy and peak spectral index. The six panels are top left: the optical luminosity at rest frame 200 s versus rest frame T90. Top right: the X-ray luminosity at rest frame 200 s versus rest frame T90. Middle left: the optical average decay index determined from rest frame 200 s versus rest frame T90. Middle right: the X-ray average decay index determined from rest frame 200 s versus rest frame T90. Bottom left: the isotropic prompt emission E_{iso} versus rest frame T90. Bottom right: the gamma-ray peak energy versus rest frame T90. In all panels, the red solid line represents the best-fitting regression and the blue dashed line represents the 3σ deviation. In the top-right corner of each panel, we give the Spearman rank coefficient, ρ, and corresponding null hypothesis probability, P, and we provide the best-fitting slope and constant determined by linear regression. We also overlaid purple pentagons on top of those data points for which the X-ray afterglow was contaminated at rest frame 200 s by the end of the prompt emission, see Section 6.3.

important that we compare the observed behaviour with that predicted from the simulations. The Monte Carlo simulation suggests we should expect a strong linear relationship between log $L_{O,200\,s}$ & log $L_{X,200\,s}$ for a sample of 48 GRBs. The observed linear regression equation is consistent with that simulated at the 1σ level. The simulation predicts a non-linear relationship between log $L_{O,200\,s}$ & log $L_{X,200\,s}$. It implies that the brighter the GRB afterglow, the greater the ratio between the X-ray and optical/UV luminosity at 200 s, such that the X-ray luminosity increases as $L_{X,200\,s} = L_{O,200\,s}^{0.82}$.

The standard afterglow model (Sari et al. 1998) also predicts several relationships linking the X-ray and optical/UV temporal indices. The exact closure relation (e.g Zhang et al. 2006; Racusin et al. 2009; Gao et al. 2013) depends on the density structure of external medium and the location of the observed spectral bands relative to the synchrotron frequencies. These relationships also relate the spectral index to the temporal index, which enable a more complete picture of the outflow to be formed. In order to obtain information about the outflow producing the afterglow emission and the medium in to which it explodes, it is preferable to examine both the temporal and spectral parameters of both the X-ray and optical/UV of each light-curve segment, as has already been explored for many GRBs (De Pasquale et al. 2006; Gendre, Corsi & Piro 2006; Starling et al. 2008; Curran et al. 2009; Schulze et al. 2011; De Pasquale et al. 2013). However, we can get an idea of the locations of the X-ray and optical/UV observing bands relative to each other and the structure of the external medium just by examining the temporal indices

of two observed frequencies. The closure relations predict that the difference between optical/UV and X-ray decay rate should either be $\Delta\alpha = 0$, if they lie on the same part of the synchrotron spectrum, or $|\Delta\alpha| = 0.25$–0.5 with a value of 0.25 if the synchrotron cooling frequency lies between the X-ray and optical bands and up to 0.5 if energy injection is also considered. The $\Delta\alpha$ is expected to be the same whether GRBs are observed on or off-axis (e.g. Margutti et al. 2010). We have added lines representing these expected differences to the bottom panel of Fig. 1. The best-fitting regression line lies above, but close to, the line $\alpha_{X,>200\,s} = \alpha_{O,>200\,s} - 0.25$. This implies that a constant density medium is preferred and the cooling frequency is likely to lie between the X-ray and optical/UV bands at least for a large number of events. This is consistent with recent analyses by Rykoff et al. (2009), Oates et al. (2011), Schulze et al. (2011) and De Pasquale et al. (2013) and supports our choice of assumptions in Sections 4 & 5. We note that, while the majority of GRBs in our sample are consistent with lying in a constant density medium, there are a few GRBs that are consistent with lying in a wind-like medium; these are some of the fastest decaying and therefore the brightest GRBs in the sample. The possibility of the most energetic GRBs having the fastest decaying afterglows and occurring in wind environments has also been briefly examined by De Pasquale et al. (2013) and will be examined in more detail in a forthcoming paper (De Pasquale et al., in preparation). We further note that the average decay index is an idealized measure of the afterglow behaviour. In reality, the light curves are likely to consist of one or more temporal segments. However, the closure relations always predict that if $\nu_m < \nu_o < \nu_c < \nu_x$, then in a wind environment we should typically see the X-ray light-curve decay more quickly than the optical/UV, in a constant density environment it is the other way round. This occurs even if energy injection is considered.

The slope of the best-fitting regression line of $\alpha_{O,>200\,s}$ versus $\alpha_{X,>200\,s}$ is consistent with being unity, suggesting that the average decay rates of the X-ray and optical/UV light curves are determined by the same mechanism. Comparing this to the Monte Carlo simulation, we see that the mean Spearman rank coefficient for the simulation is similar to that determined for the observed data, 32.9 per cent of the simulated sample have Spearman rank coefficients equal to or greater than that observed, indicating that the observed relationship is fully consistent with that expected from the standard afterglow model. We also find that the slopes and constant parameters of the observed linear regression for $\alpha_{O,>200\,s}$ versus $\alpha_{X,>200\,s}$ are consistent within 1σ with those simulated. This suggests that the observed relationship between $\alpha_{O,>200\,s}$ and $\alpha_{X,>200\,s}$ is consistent with the prediction of the standard afterglow model.

We also examined the relationship between log $L_{200\,s}$ versus $\alpha_{>200\,s}$. For both the optical/UV and X-ray, we find the linear regressions give relationships that are consistent at 1σ. This suggests that the same mechanism is producing both correlations. Comparing the observations with the simulations, we find 0.0 per cent of the 10 000 simulations have Spearman rank coefficients more negative or equal to that observed. Similarly only 1.5 per cent of the simulations have Spearman rank coefficients equal to or more negative than that observed for the log $L_{O,200\,s}$ versus $\alpha_{O,>200\,s}$ correlation. Comparing the linear regression parameters for the observed and predicted data, we find that the slopes and constant parameters are inconsistent at $\gtrsim 4\sigma$. Since the average values of the simulated distributions of log $L_{200\,s}$ and $\alpha_{>200\,s}$ are consistent with the mean values of the observed parameter distributions, this indicates that we are simulating GRBs that are representative of our observed sample. Therefore, this implies that correlations as strong as those

observed for both the X-ray and optical/UV light curves should not be expected to be present in our observed sample.

The standard afterglow model also predicts correlations between the isotropic energy log E_{iso} with the afterglow luminosity log $L_{200\,s}$, see equation (2). Since we see a large fraction of GRBs consistent with the cooling frequency lying in between the X-ray and optical/UV bands (e.g bottom panel of Fig. 1), we may expect the X-ray points to predominately satisfy the second equation and the optical/UV predominately satisfy the first relation. Yet, the simulation suggests that a single relationship can explain the optical/UV and X-ray correlations between log E_{iso} and log $L_{200\,s}$ as the simulated slopes are consistent to within 1σ, which is in agreement with the observed sample. However, we further examined the log $L_{200\,s}$ and log E_{iso} correlation by directly comparing the slopes of the simulations and observations. We find them to be inconsistent at $\gtrsim 3\sigma$, with the slope of the observed relationship being much shallower than that predicted by the simulation.

Spearman rank correlation of the simulated log E_{iso} and log $L_{200\,s}$ also suggests that we should be observing weaker correlations in comparison to what we observe, with 0.3 and 0.06 per cent of the simulations having Spearman rank coefficients equal to or larger than that observed for the optical/UV and X-ray, respectively. This is likely related to our choice of efficiency. A wide range in efficiency is likely to introduce more scatter in the relationship between log E_{iso} and log $L_{200\,s}$. To explore what effect a narrower efficiency would have, we repeated our simulation with the efficiency parameter fixed at 0.1 and then again at 0.9. In both cases, we found the simulated Spearman rank correlation values were more consistent with those observed, suggesting that the observed sample has a relatively narrow range in efficiency. However, the slopes of the simulated and observed relationships remain inconsistent at $\gtrsim 3\sigma$ when fixing the efficiency parameter.

In Section 4, we also determined the expected relationship between the ratio (L_O/L_X) and E_k. We showed that the expected range in the ratio should lie between 1.05 and 3.16. Comparing these predictions with Fig. 3, we see that the observed values are consistent with this range and therefore consistent with the standard afterglow model. We also note that we do not see evidence for or against evolution of this ratio with energy as predicted by the second relationship in equation (3), however we should not expect to observe a strong correlation because the evolution is very shallow as indicated by the dotted line in Fig. 3.

Finally, we also observe that the observed relationships between log E_{iso} and $\alpha_{>200\,s}$ for the X-ray and optical/UV are consistent at 1σ. We find that only 0.01 per cent of the simulations predict the same or stronger relationship between log E_{iso} and $\alpha_{X,>200\,s}$ and 0.03 per cent of simulations predict similar or stronger relationship between log E_{iso} and $\alpha_{O,>200\,s}$. The slopes and constant parameters for the linear regression from the simulation are inconsistent with the observed data at $\gtrsim 2.3\sigma$. This suggests that the relationships given in Table 2, for both the X-ray and optical/UV light curves, between log E_{iso} and $\alpha_{>200\,s}$ are not expected in the standard afterglow model. The lack of strong correlation predicted by the simulation is to be expected since the temporal slopes given by the closure relations (e.g. Zhang et al. 2006; Racusin et al. 2009) are a function of the electron energy index only and are not seemingly directly related to the energy of the outflow.

Overall, we would expect to see relationships observed between log $L_{O,200\,s}$ & log $L_{X,200\,s}$ and $\alpha_{O,>200\,s}$ versus $\alpha_{X,>200\,s}$ arise because the same afterglow is observed in both the X-ray and optical/UV. These relationships can be explained easily by the standard afterglow model and are fully consistent with our simulations.

Also a relationship between log E_{iso} versus log $L_{200\,s}$ is expected in the standard afterglow model, however, comparison of our observed relationship to the simulations suggests that the observed linear regression slope is less steep than predicted by the simulation. Furthermore, the relationships we observe, between log $L_{200\,s}$ and $\alpha_{>200\,s}$, and log E_{iso} and $\alpha_{>200\,s}$, are not predicted by the simulations and are not expected in the standard afterglow model. Since the standard afterglow does not succeed in fully predicting all of our observed correlations, it is therefore likely that a more complex outflow model is required. This conclusion is similar to that drawn during the separate investigation of the optical/UV log $L_{200\,s}$-$\alpha_{>200\,s}$ decay correlation.

To summarize, we find that the optical/UV and X-ray afterglows are strongly related and it is likely that they are produced by the same outflow and by the same or at least related mechanisms. However, as indicated above the basic standard afterglow model does not predict all of our observed correlations and it is therefore likely that a more complex outflow model is required to explain all the observed correlations.

7.2 Alternative models

There are two main possibilities that could make the outflow complex enough to be able to reproduce the observed correlations. The first is that perhaps there is some mechanism or parameter that controls the amount of energy given to and distributed during the prompt and afterglow phases and that also regulates the afterglow decay rate. This should occur in such a way that for events with the largest gamma-ray isotropic energy, the energy given to the afterglow is released quickly, resulting in an initially bright afterglow which decays rapidly. Conversely, if the gamma-ray isotropic energy is smaller, then the afterglow energy is released slowly over a longer period, the afterglow will be less bright initially and decay at a slower rate.

The second possibility is that the correlations could be a geometric effect, perhaps the result of the observer's viewing angle. Jets viewed away from the jet-axis may have fainter afterglows that decay less quickly in comparison to afterglows viewed closer to the centre of the jet (see fig 3. of Panaitescu & Vestrand 2008). Similarly, this will also affect the observed prompt emission, with jets viewed off-axis appearing to have lower isotropic energy and lower peak spectral energy (Ramirez-Ruiz et al. 2005). In this case, the relationship between luminosity and decay rate of GRB afterglow light curves should be observed in uniform jets and in structured outflows (Panaitescu & Vestrand 2008). By looking at fig. 3 of Panaitescu & Vestrand (2008), two further tests can be derived to determine if this scenario is producing the observed afterglows. The first is that we should expect to see convergence of the light curves at late times to a similar decay rate for all observing angles when the emission from the entire jet is observed by the observer. The convergence time and the range of decay rates will vary, depending on how the outflow is structured. The second is that afterglows that are viewed more off-axis will rise later. Therefore, we should also observe a correlation between afterglow brightness and peak time, although the strength of this correlation will be affected by whether or not GRBs have similar jet structure. This latter test has been explored by Panaitescu & Vestrand (2008), Panaitescu & Vestrand (2011) and Panaitescu et al. (2013). They find a significant correlation between the peak time and peak afterglow brightness in both the X-ray and optical light curves consistent with this hypothesis. However, we note that this correlation was determined from GRBs with observed

rises and therefore afterglows that peak before observations begin will not have been included (Panaitescu et al. 2013).

8 CONCLUSIONS

In the optical/UV GRB afterglow sample of Oates et al. (2012), a correlation was found between the early optical/UV luminosity (measured at rest frame 200 s, log $L_{200\,s}$) and average decay rate (measured from 200 s, $\alpha_{>200\,s}$). The aim of this paper was to explore whether this was also observed in the X-ray light curves, to explore how this correlation relates to the prompt emission phase and to explore if what we see is consistent with the predictions of the standard afterglow model.

We first began by exploring what relationships the standard afterglow model predicts for our observed parameters. For different ordering of the spectral frequencies, this model predicts more than one expression for the relationship between two parameters. It is therefore not possible to analytically predict the expected correlations for a sample of GRBs with a mixture of spectral regimes. Therefore, we performed a Monte Carlo simulation to predict the relationships between various combinations of parameters for a sample of 48 GRBs.

We then examined the afterglow parameters and correlations resulting from the observed sample and compared them to the prediction of the simulations. We find luminosity–decay correlations in both the optical/UV and X-ray light curves and find that these relationships are consistent (see also Racusin et al. 2015). This suggests a single underlying mechanism producing the correlations in both bands, regardless of their detailed temporal behaviour. We also show significant correlations between the logarithmic X-ray and optical/UV luminosity (log $L_{O,200\,s}$, log $L_{X,200\,s}$) and the optical/UV and X-ray decay indices ($\alpha_{O,>200\,s}$ and $\alpha_{X,>200\,s}$). These relationships are predicted by the standard afterglow model and the observations are consistent with our simulations. However, such strong correlations between log $L_{200\,s}$ and $\alpha_{>200\,s}$ at both wavelengths are not predicted in the standard afterglow model and are inconsistent with our simulations.

Finally, we compared the parameters in the both the X-ray and optical/UV luminosity–decay correlations with the prompt emission parameters, such as isotropic energy (E_{iso}), rest-frame peak spectral energy (E_{peak}) and the rest-frame T90 parameter (duration over which 90 per cent of the emission is observed). We show significant evidence that the X-ray and optical luminosities, measured at 200 s, are correlated with E_{iso} and slightly less strongly correlated with E_{peak}. This is consistent with previous findings (e.g. D'Avanzo et al. 2012; Margutti et al. 2013) and predictions of the standard afterglow model and our simulations, although the slopes of the relationships between luminosity and isotropic energy are steeper in the simulations than observed. The average decay indices for the X-ray and optical/UV bands are also correlated with E_{iso}, but these co-slightly weaker in comparison to the correlations observed for the luminosities at 200 s and E_{iso}. The observed relationships between $\alpha_{>200\,s}$ and E_{iso} are not expected in the standard afterglow model and are inconsistent with our simulations.

Together these correlations imply that the GRBs with the brightest afterglows in the X-ray and optical bands, decay the fastest and they also have the largest observed prompt emission energies and typically larger peak spectral energy. This suggests that what happens during the prompt phase has direct implications on the afterglow.

Overall, while correlations between the luminosities in both the X-ray and optical/UV bands, between the decay indices and

between the luminosities and the isotropic energy are predicted by the simulation of the standard afterglow model, observed relationships involving the average decay indices with either luminosity at 200 s or the isotropic energy are not consistent with the standard afterglow model. We therefore suggest that a more complex afterglow or outflow model is required to produce all the observed correlations. This may be due to either a viewing angle effect or by some mechanism or physical property controlling the energy release within the outflow.

ACKNOWLEDGEMENTS

REFERENCES

Amati L., 2006, MNRAS, 372, 233
Amati L. et al., 2002, A&A, 390, 81
Band D., Matteson J., Ford L., Schaefer B., Palmer D., Teegarden B., Cline T., Briggs M., 1993, ApJ, 413, 281
Berger E., Kulkarni S. R., Frail D. A., 2003, ApJ, 590, 379
Berger E., Fox D. B., Cucchiara A., Cenko S. B., 2008, GCN Circ., 8335, 1
Bernardini M. G., Margutti R., Mao J., Zaninoni E., Chincarini G., 2012, A&A, 539, A3
Bloom J. S., Frail D. A., Sari R., 2001, AJ, 121, 2879
Bloom J. S., Perley D. A., Chen H. W., 2006, GCN Circ., 5826
Boër M., Gendre B., 2000, A&A, 361, L21
Cenko S. B. et al., 2009a, ApJ, 693, 1484
Cenko S. B., Perley D. A., Junkkarinen V., Burbidge M., Diego U. S., Miller K., 2009b, GCN Circ., 9518, 1
Chen H.-W., Helsby J., Shectman S., Thompson I., Crane J., 2009, GCN Circ., 10038, 1
Chornock R., Cenko S. B., Griffith C. V., Kislak M. E., Kleiser I. K. W., Filippenko A. V., 2009a, GCN Circ., 9151, 1
Chornock R., Perley D. A., Cenko S. B., Bloom J. S., 2009b, GCN Circ., 9243, 1
Chornock R., Perley D. A., Cobb B. E., 2009c, GCN Circ., 10100, 1
Chornock R., Berger E., Fox D., Levan A. J., Tanvir N. R., Wiersema K., 2010, GCN Circ., 11164, 1
Cucchiara A., Fox D. B., 2008, GCN Circ., 7654, 1
Cucchiara A., Fox D. B., Cenko S. B., Berger E., 2008a, GCN Circ., 8346, 1
Cucchiara A., Fox D. B., Cenko S. B., Berger E., 2008b, GCN Circ., 8713, 1
Curran P. A., Starling R. L. C., van der Horst A. J., Wijers R. A. M. J., 2009, MNRAS, 395, 580
D'Avanzo P. et al., 2012, MNRAS, 425, 506
D'Elia V. et al., 2005, GCN Circ., 3746, 1
Dainotti M. G., Cardone V. F., Capozziello S., 2008, MNRAS, 391, L79
De Pasquale M. et al., 2006, A&A, 455, 813
De Pasquale M., Schulze S., Kann D. A., Oates S., Zhang B., 2013, in Castro-Tirado A. J., Gorosabel J., Park I. H., eds, EAS Publ. Ser. Vol. 61, Gamma-ray Bursts: 15 Years of GRB Afterglows. p. 217
de Ugarte Postigo A., Gorosabel J., Fynbo J. P. U., Wiersema K., Tanvir N., 2009, GCN Circ., 9771, 1
de Ugarte Postigo A. et al., 2011, GCN Circ., 11579, 1

Evans P. A. et al., 2007, A&A, 469, 379
Evans P. A. et al., 2009, MNRAS, 397, 1177
Feigelson E. D., Babu G. J., 1992, ApJ, 397, 55
Ferrero P. et al., 2009, A&A, 497, 729
Foley R. J., Chen H.-W., Bloom J., Prochaska J. X., 2005, GCN Circ., 3483
Fox A. J., Ledoux C., Vreeswijk P. M., Smette A., Jaunsen A. O., 2008, A&A, 491, 189
Fynbo J. P. U. et al., 2005, GCN Circ., 3749
Fynbo J. P. U., Malesani D., Hjorth J., Sollerman J., Thoene C. C., 2008, GCN Circ., 8254, 1
Fynbo J. P. U. et al., 2009, ApJS, 185, 526
Gao H., Lei W.-H., Zou Y.-C., Wu X.-F., Zhang B., 2013, New Astron. Rev., 57, 141
Gendre B., Boër M., 2005, A&A, 430, 465
Gendre B., Corsi A., Piro L., 2006, A&A, 455, 803
Gendre B., Galli A., Boër M., 2008, ApJ, 683, 620
Gendre B., Pelisson S., Boër M., Basa S., Mazure A., 2008, A&A, 492, L1
Ghirlanda G., Ghisellini G., Lazzati D., 2004, ApJ, 616, 331
Goldstein A. et al., 2012, ApJS, 199, 19
Golenetskii S., Aptekar R., Mazets E., Pal'Shin V., Frederiks D., Ulanov M., Cline T., 2006a, GCN Circ., 4989, 1
Golenetskii S., Aptekar R., Mazets E., Pal'Shin V., Frederiks D., Cline T., 2006b, GCN Circ., 5113, 1
Golenetskii S., Aptekar R., Mazets E., Pal'Shin V., Frederiks D., Cline T., 2006c, GCN Circ., 5722
Golenetskii S., Aptekar R., Mazets E., Pal'Shin V., Frederiks D., Cline T., 2006d, GCN Circ., 5748
Golenetskii S., Aptekar R., Mazets E., Pal'Shin V., Frederiks D., Cline T., 2006e, GCN Circ., 5837
Golenetskii S., Aptekar R., Mazets E., Pal'Shin V., Frederiks D., Cline T., 2008a, GCN Circ., 7482, 1
Golenetskii S. et al., 2008b, GCN Circ., 7995, 1
Golenetskii S. et al., 2009a, GCN Circ., 9083, 1
Golenetskii S., Aptekar R., Mazets E., Pal'Shin V., Frederiks D., Oleynik P., Ulanov M., Svinkin D., 2009b, GCN Circ., 10045, 1
Golenetskii S. et al., 2010, GCN Circ., 11251, 1
Gruber D. et al., 2014, ApJS, 211, 12
Isobe T., Feigelson E. D., Akritas M. G., Babu G. J., 1990, ApJ, 364, 104
Jakobsson P. et al., 2006a, A&A, 460, L13
Jakobsson P., Levan A., Chapman R., Rol E., Tanvir N., Vreeswijk P., Watson D., 2006b, GCN Circ., 5617
Jakobsson P., Fynbo J. P. U., Tanvir N., Rol E., 2006c, GCN Circ., 5716
Jakobsson P., Fynbo J. P. U., Vreeswijk P. M., Malesani D., Sollerman J., 2007, GCN Circ., 7076, 1
Jakobsson P. et al., 2008, GCN Circ., 7998, 1
Jaunsen A. O., Fynbo J. P. U., Andersen M. I., Vreeswijk P., 2007, GCN Circ., 6216
Kann D. A. et al., 2010, ApJ, 720, 1513
Kendall M., Stuart A., 1979, The Advanced Theory of Statistics. Vol.2: Inference and Relationship. Griffin, London
Kouveliotou C. et al., 2004, ApJ, 608, 872
Kuin N. P. M. et al., 2009, MNRAS, 395, L21
Lazzati D., Morsony B. J., Margutti R., Begelman M. C., 2013, ApJ, 765, 103
Li L. et al., 2012, ApJ, 758, 27
Liang E., Zhang B., 2006, ApJ, 638, L67
Liang E.-W. et al., 2013, ApJ, 774, 13
Margutti R. et al., 2010, MNRAS, 402, 46
Margutti R. et al., 2013, MNRAS, 428, 729
Melandri A. et al., 2008, ApJ, 686, 1209
Melandri A. et al., 2014, A&A, 565, A72
Nardini M., Ghisellini G., Ghirlanda G., Tavecchio F., Firmani C., Lazzati D., 2006, A&A, 451, 821
Nardini M., Ghisellini G., Ghirlanda G., 2008, MNRAS, 386, L87
Nysewander M., Fruchter A. S., Pe'er A., 2009, ApJ, 701, 824
Oates S. R. et al., 2007, MNRAS, 380, 270

Oates S. R. et al., 2009, MNRAS, 395, 490

Oates S. R. et al., 2011, MNRAS, 412, 561

Oates S. R., Page M. J., De Pasquale M., Schady P., Breeveld A. A., Holland S. T., Kuin N. P. M., Marshall F. E., 2012, MNRAS, 426, L86

Paciesas W. S. et al., 2012, ApJS, 199, 18

Panaitescu A., Kumar P., 2000, ApJ, 543, 66

Panaitescu A., Vestrand W. T., 2008, MNRAS, 387, 497

Panaitescu A., Vestrand W. T., 2011, MNRAS, 414, 3537

Panaitescu A., Vestrand W. T., Woźniak P., 2013, MNRAS, 433, 759

Press W. H., Teukolsky S. A., Vetterling W. T., Flannery B. P., 1992, Numerical recipes in C. The art of scientific computing

Prochaska J. X., Murphy M., Malec A. L., Miller K., 2008, GCN Circ., 7388, 1

Racusin J. L. et al., 2009, ApJ, 698, 43

Racusin J. L., Oates S. R., De Pasquale M., Kocevski D., 2015, ApJ, submitted

Ramirez-Ruiz E., Granot J., Kouveliotou C., Woosley S. E., Patel S. K., Mazzali P. A., 2005, ApJ, 625, L91

Rol E., Jakobsson P., Tanvir N., Levan A., 2006, GCN Circ., 5555

Roming P. W. A. et al., 2005, Space Sci. Rev., 120, 95

Rykoff E. S. et al., 2009, ApJ, 702, 489

Sakamoto T. et al., 2009, ApJ, 693, 922

Sakamoto T. et al., 2011, ApJS, 195, 2

Sari R., Piran T., Narayan R., 1998, ApJ, 497, L17

Schady P. et al., 2010, MNRAS, 401, 2773

Schulze S. et al., 2011, A&A, 526, A23

Starling R., Thoene C. C., Fynbo J. P. U., Vreeswijk P., Hjorth J., 2006, GCN Circ., 5131, 1

Starling R. L. C., van der Horst A. J., Rol E., Wijers R. A. M. J., Kouveliotou C., Wiersema K., Curran P. A., Weltevrede P., 2008, ApJ, 672, 433

Tanvir N. R., Wiersema K., Levan A. J., 2010, GCN Circ., 11230, 1

Thoene C. C. et al., 2006, GCN Circ., 5373, 1

Thoene C. C., de Ugarte Postigo A., Vreeswijk P. M., Malesani D., Jakobsson P., 2008, GCN Circ., 8058, 1

Vergani S. D. et al., 2010, GCN Circ., 10495, 1

Vreeswijk P., Jaunsen A., 2006, GCN Circ., 4974, 1

Vreeswijk P. M., Smette A., Malesani D., Fynbo J. P. U., Milvang-Jensen B., Jakobsson P., Jaunsen A. O., Ledoux C., 2008a, GCN Circ., 7444, 1

Vreeswijk P. M., Thoene C. C., Malesani D., Fynbo J. P. U., Hjorth J., Jakobsson P., Tanvir N. R., Levan A. J., 2008b, GCN Circ., 7601, 1

Vreeswijk P., Malesani D., Fynbo J., Jakobsson P., Thoene C., Sollerman J., Watson D., Milvang-Jensen B., 2008c, GCN Circ., 8301, 1

Wiersema K., Tanvir N. R., Cucchiara A., Levan A. J., Fox D., 2009, GCN Circ., 10263, 1

Xu D. et al., 2009, GCN Circ., 10053, 1

Zaninoni E., Grazia Bernardini M., Margutti R., Oates S., Chincarini G., 2013, A&A, 557, A12

Zhang B., Kobayashi S., Mészáros P., 2003, ApJ, 595, 950

Zhang B., Fan Y. Z., Dyks J., Kobayashi S., Mészáros P., Burrows D. N., Nousek J. A., Gehrels N., 2006, ApJ, 642, 354

Zhang B. et al., 2007, ApJ, 655, 989

APPENDIX A

Table A1. Table containing all the parameters for all the GRBs in the sample: X-ray and optical luminosity at rest frame 200 s $\log L_{200\,s}$, average decay indices of the X-ray and optical/UV light curves measured using data from rest frame 200 s, $\alpha_{>200\,s}$; and observer frame values for isotropic energy E_{iso}, gamma-ray peak energy E_{peak}, and duration of the prompt emission. For E_{peak}, where no reference is given we used the correlation between the peak energy and the photon index of the νF_{ν} spectrum to estimate E_{peak} (see Sakamoto et al. 2009, for further details). The relationship can only be used to estimate E_{peak} when the power-law index of the BAT spectrum is between -2.3 and -1.3, which places E_{peak} approximately within the BAT range. References: 1) Jakobsson et al. (2006a),2) Foley et al. (2005), 3) Fynbo et al. (2009), 4) D'Elia et al. (2005), 5) Oates et al. (2012), 6) Fynbo et al. (2005), 7) Vreeswijk & Jaunsen (2006), 8) Oates et al. (2012), 9) Starling et al. (2006), 10) Ferrero et al. (2009), 11) Fox et al. (2008), 12) Thoene et al. (2006), 13) Rol et al. (2006), 14) Jakobsson et al. (2006b), 15) Jakobsson et al. (2006c), 16) Bloom, Perley & Chen (2006), 17) Jaunsen et al. (2007), 18) Jakobsson et al. (2007), 19) Prochaska et al. (2008), 20) Vreeswijk et al. (2008a), 21) Vreeswijk et al. (2008b), 22) Cucchiara & Fox (2008), 23) Jakobsson et al. (2008), 24) Thoene et al. (2008), 25) Fynbo et al. (2008), 26) Vreeswijk et al. (2008c), 27) Berger et al. (2008), 28) Cucchiara et al. (2008a), 29) Kuin et al. (2009), 30) Cucchiara et al. (2008b), 31) Chornock et al. (2009a), 32) Chornock et al. (2009b), 33) Cenko et al. (2009b), 34) de Ugarte Postigo et al. (2009), 35) Chen et al. (2009), 36) Xu et al. (2009), 37) Chornock, Perley & Cobb (2009c), 38) Wiersema et al. (2009), 39) Vergani et al. (2010), 40) Chornock et al. (2010), 41) Tanvir, Wiersema & Levan (2010), 42) de Ugarte Postigo et al. (2011). [a]Sakamoto et al. (2011), [b]Golenetskii et al. (2006a), [c]Golenetskii et al. (2006b), [d]Golenetskii et al. (2006c), [e]Golenetskii et al. (2006d), [f]Golenetskii et al. (2006e), [g]Golenetskii et al. (2008a), [h]Golenetskii et al. (2008b), [i]Goldstein et al. (2012), [j]Gruber et al. (2014), [k]Golenetskii et al. (2009a), [l]Golenetskii et al. (2009b), [m]Golenetskii et al. (2010).

GRB	Redshift	$\log L_{O,200\,s}$	$\log L_{X,200\,s}$	$\alpha_{O,>200\,s}$	$\alpha_{X,>200\,s}$	$\log E_{iso}$	E_{peak}	T90
GRB050319	3.2425[1]	31.84 ± 0.26	29.76 ± 0.08	−0.68 ± 0.06	−0.84 ± 0.02	52.71	45	151.7
GRB050525A	0.606[2]	31.30 ± 0.04	29.82 ± 0.09	−1.10 ± 0.01	−1.53 ± 0.04	52.42	80[a]	8.8
GRB050730	3.9693[3,4]	32.75 ± 0.08	31.16 ± 0.02	−1.31 ± 0.11	−2.00 ± 0.02	53.14	101	145.1
GRB050801	1.38[3,5]	31.68 ± 0.02	29.29 ± 0.11	−1.28 ± 0.10	−1.15 ± 0.04	51.42	40	19.4
GRB050802	1.71[6]	31.89 ± 0.09	30.24 ± 0.06	−0.80 ± 0.03	−1.18 ± 0.01	52.51	107	27.5
GRB050922C	2.1995[1]	32.40 ± 0.05	30.52 ± 0.03	−1.03 ± 0.03	−1.30 ± 0.02	52.60	136	4.5
GRB060418	1.49[7]	32.60 ± 0.01	30.50 ± 0.02	−1.24 ± 0.01	−1.40 ± 0.02	53.14	230[b]	109.2
GRB060510A	1.2[8]	32.11 ± 0.05	30.08 ± 0.04	−0.48 ± 0.05	−1.01 ± 0.01	52.89	184[c]	20.2
GRB060512	2.100[3,9]	31.70 ± 0.06	30.13 ± 0.09	−1.05 ± 0.05	−1.17 ± 0.05	51.86	−	11.4
GRB060526	3.2213[1]	32.26 ± 0.10	29.94 ± 0.09	−0.87 ± 0.06	−0.99 ± 0.03	52.67	44	275.2
GRB060605	3.773[10]	32.91 ± 0.12	30.27 ± 0.08	−1.15 ± 0.11	−1.57 ± 0.04	52.86	148	539.1
GRB060607A	3.0749[11]	32.62 ± 0.05	30.79 ± 0.03	−1.20 ± 0.06	−1.59 ± 0.02	53.01	114	103.0
GRB060708	1.92[5]	31.50 ± 0.14	29.74 ± 0.05	−0.82 ± 0.35	−1.17 ± 0.02	51.92	79	10.0
GRB060729	0.5428[3,12]	30.23 ± 0.08	28.74 ± 0.04	−0.63 ± 0.01	−0.82 ± 0.01	51.55	72	113.0
GRB060908	1.8836[13]	31.53 ± 0.10	30.28 ± 0.07	−1.14 ± 0.13	−1.46 ± 0.05	52.74	148[a]	18.8
GRB060912A	0.937[14]	31.04 ± 0.16	29.00 ± 0.06	−0.55 ± 0.05	−1.10 ± 0.03	51.75	67	5.0
GRB061007	1.262[15]	33.28 ± 0.02	31.05 ± 0.01	−1.60 ± 0.02	−1.68 ± 0.01	53.91	399[d]	75.7

Table A1 – *continued*

GRB	Redshift	log $L_{O,200s}$	log $L_{X,200s}$	$\alpha_{O,>200s}$	$\alpha_{X,>200s}$	log E_{iso}	E_{peak}	T90
GRB061021	0.346[3]	30.27 ± 0.04	28.50 ± 0.06	−0.86 ± 0.01	−0.95 ± 0.01	51.82	778[e]	43.8
GRB061121	1.314[16]	31.88 ± 0.09	30.10 ± 0.02	−0.70 ± 0.02	−1.09 ± 0.01	53.55	606[f]	81.2
GRB070318	0.8397[3,17]	31.97 ± 0.05	29.53 ± 0.03	−1.00 ± 0.02	−1.17 ± 0.02	52.02	130	131.5
GRB071112C	0.823[18]	31.00 ± 0.06	29.48 ± 0.03	−1.23 ± 0.07	−1.45 ± 0.02	–	–	44.80
GRB080310	2.4274[3,19]	31.90 ± 0.11	29.39 ± 0.08	−0.89 ± 0.04	−1.13 ± 0.03	52.76	26	352.4
GRB080319B	0.9382[3,20]	33.01 ± 0.03	31.49 ± 0.01	−1.48 ± 0.01	−1.64 ± 0.01	54.07	651[g]	124.9
GRB080413B	1.1014[3,21]	31.67 ± 0.14	29.88 ± 0.04	−0.73 ± 0.04	−1.02 ± 0.01	52.27	78[a]	8.0
GRB080430	0.767[22]	30.46 ± 0.08	28.73 ± 0.04	−0.70 ± 0.03	−0.78 ± 0.01	51.51	66	14.2
GRB080721	2.5914[3,23]	32.93 ± 0.09	31.61 ± 0.01	−1.14 ± 0.05	−1.40 ± 0.01	54.01	485[h]	176.3
GRB080804	2.2045[24]	31.67 ± 0.04	29.80 ± 0.06	−0.94 ± 0.03	−1.11 ± 0.02	52.94	109[i,j]	37.2
GRB080810	3.3604[3]	33.34 ± 0.10	30.61 ± 0.03	−1.16 ± 0.09	−1.58 ± 0.03	53.84	856[i,j]	107.7
GRB080916A	0.689[25]	31.08 ± 0.19	28.97 ± 0.06	−0.79 ± 0.06	−0.97 ± 0.02	52.05	129[a]	61.3
GRB080928	1.6919[3,26]	31.06 ± 0.19	30.05 ± 0.05	−1.29 ± 0.06	−1.55 ± 0.04	52.49	67	233.7
GRB081007	0.5295[27]	30.20 ± 0.06	28.69 ± 0.09	−0.70 ± 0.02	−0.88 ± 0.01	51.06	–	9.0
GRB081008	1.967[28]	32.82 ± 0.08	30.10 ± 0.02	−1.09 ± 0.02	−1.25 ± 0.02	53.06	229[i,j]	179.5
GRB081203A	2.100[29]	33.55 ± 0.02	30.60 ± 0.02	−1.52 ± 0.01	−1.43 ± 0.02	53.21	119	223.0
GRB081222	2.77[30]	32.46 ± 0.04	30.93 ± 0.02	−0.93 ± 0.03	−1.22 ± 0.01	53.27	143[i,j]	33.0
GRB090401B	3.1[5]	32.49 ± 0.01	31.37 ± 0.01	−1.71 ± 0.16	−1.45 ± 0.01	54.01	409[k]	186.5
GRB090418A	1.608[31]	33.13 ± 0.15	30.29 ± 0.07	−1.18 ± 0.22	−1.27 ± 0.02	52.83	142	56.3
GRB090424	0.544[32]	31.64 ± 0.07	30.12 ± 0.01	−0.75 ± 0.02	−1.11 ± 0.01	52.56	154[a]	49.5
GRB090618	0.54[33]	31.59 ± 0.01	30.09 ± 0.01	−0.99 ± 0.01	−1.41 ± 0.01	53.41	147[i,j]	113.3
GRB090812	2.452[34]	32.42 ± 0.13	30.69 ± 0.02	−1.19 ± 0.35	−1.16 ± 0.02	53.97	–	75.1
GRB091018	0.971[35]	31.69 ± 0.02	29.85 ± 0.03	−0.96 ± 0.01	−1.18 ± 0.01	51.79	28[l]	4.4
GRB091020	1.71[36]	33.06 ± 0.10	30.35 ± 0.03	−1.17 ± 0.06	−1.20 ± 0.01	52.92	244[i,j]	38.9
GRB091029	2.752[37]	31.54 ± 0.11	30.01 ± 0.05	−0.72 ± 0.02	−0.81 ± 0.01	52.85	61[a]	39.2
GRB091208B	1.063[38]	31.69 ± 0.21	29.69 ± 0.06	−0.79 ± 0.09	−1.06 ± 0.02	52.31	127[i,j]	14.8
GRB100316B	1.180[39]	31.31 ± 0.12	29.07 ± 0.13	−0.94 ± 0.09	−1.09 ± 0.06	51.12	25	3.9
GRB100805A	1.85[5]	32.11 ± 0.11	29.40 ± 0.08	−0.73 ± 0.12	−1.63 ± 0.02	51.88	64	16.6
GRB100901A	1.408[40]	31.36 ± 0.05	28.07 ± 0.09	−0.62 ± 0.01	−1.02 ± 0.02	52.26	80	436.4
GRB100906A	1.727[41]	32.83 ± 0.02	30.06 ± 0.03	−1.13 ± 0.01	−1.30 ± 0.02	53.57	142[m]	114.3
GRB101219B	0.5519[42]	30.56 ± 0.08	27.47 ± 0.13	−0.82 ± 0.04	−0.65 ± 0.03	51.59	83[i,j]	42.0

This paper has been typeset from a TEX/LATEX file prepared by the author.